



Recent Advancements and Perspective of High-Performance Printed Power Sources with Multiple Form Factors

Xiaoyu Shi^{1,2,3} · Zhong-Shuai Wu¹ · Xinhe Bao^{1,2}

Received: 7 January 2020 / Revised: 13 April 2020 / Accepted: 8 May 2020 / Published online: 3 June 2020
© Shanghai University and Periodicals Agency of Shanghai University 2020

Abstract

The rapid development of wearable and smart electronics for environmental sensors, Internet of things and implantable medical devices has accelerated the demand for high-performance electrochemical energy storage devices (EESDs) that possess high safety and diverse form factors. Of these devices, printable EESDs including batteries and supercapacitors are regarded as a novel class of highly competitive candidates to meet the demands to future wearable, portable and integrated power sources due to their low costs, scalability and outstanding compatibility with industrial processes. In addition, printable EESDs can enable the design of various form factors, including tailored sizes and shapes, miniaturization, flexibility, esthetic versatility and integration. Based on this, this review will provide a topical overview of recent advancements in printable EESDs with a focus on representative printing techniques and their intriguing features, including rheological requirements to component inks, printing resolutions, compatible substrates and potential applications for the fabrication of high-performance EESDs. This review will also discuss the diversified form factors and functionalities of printable EESDs that allow for designable shapes, mechanical robustness and integration toward unconventional, customized, flexible and smart applications in future electronics and present the existing challenges and perspective of printed power sources with multiple form factors.

Keywords Printing technique · Energy storage · Battery · Supercapacitor · Form factor

1 Introduction

The rapid development of wearable and smart electronics has led to increasing demands for high-performance electrochemical energy storage devices (EESDs) including rechargeable batteries and supercapacitors (SCs) that possess high energy densities, fast charge-discharge rates, enhanced safety features and long-term cycling life spans [1–7]. In addition, viable next-generation EESDs need to

possess diversified form factors, including the possibility for miniaturization and integration as well as being lightweight, flexible and esthetically pleasing to match innovative, portable and wearable electronics such as smart watches, foldable phones, microscale sensors and patchable health monitors [8–11]. In order to achieve these requirements, great efforts have been devoted to the development of key components including electrode materials (e.g., lithium metal anodes, lithium-rich cathodes) [12–16], electrolytes (e.g., solvent-in-salt electrolytes, ionic liquid electrolytes, solid-state electrolytes) [17–23], device configurations (e.g., 2D in-plane geometry, 3D array architecture) [24–26] and new EESD systems (e.g., redox-mediator supercapacitors, aqueous batteries, lithium–sulfur (Li–S) batteries, metal–air batteries) [27–32] to enhance the electrochemical performance of EESDs. However, due to the increasing demands of next-generation electronics with diversified form factors, a comprehensive understanding of electrode materials, electrolytes, device structures, current collectors, substrates and device encapsulation methods remains lacking, meaning that laboratory results achieved for EESDs cannot be

✉ Zhong-Shuai Wu
wuzs@dicp.ac.cn

¹ Dalian National Laboratory for Clean Energy, Dalian Institute of Chemical Physics, Chinese Academy of Sciences, 457 Zhongshan Road, Dalian 116023, China

² State Key Laboratory of Catalysis, Dalian Institute of Chemical Physics, Chinese Academy of Sciences, 457 Zhongshan Road, Dalian 116023, China

³ Department of Chemical Physics, University of Science and Technology of China, 96 Jinzhai Road, Hefei 230026, China

extended to industrial production as EESDs fabricated using traditional blade coating methods usually suffer from heavy weights, bulky volumes, poor mechanical properties and inferior shape customizations [11, 33–36]. And a series of fabrication methods have been developed to prepare EESDs, including photolithography [25, 37, 38], sputtering [39], plasma etching [40–43], laser scribing [44–46], electrodeposition [47, 48], vacuum filtration [49–51] and photochemical techniques [52]. However, these methods are generally limited by the need for expensive equipment, complex multi-step processes and severe work environments (e.g., photolithography, sputtering, plasma etching) [40], large waste of active material (e.g., laser scribing) [53], low efficiency (e.g., vacuum filtration) [49] or limited selection of active materials (e.g., electrodeposition, photochemical reduction) [48, 52], all of which can hardly satisfy the demands of future EESDs towards practical application. Therefore, the development of simple, efficient, cost-effective and scalable strategies for the fabrication of high-performance EESDs with various form factors is urgently needed. Here, printing technologies such as spray coating, inkjet printing, screen printing and three-dimensional (3D) printing have recently gained increasing attention as a promising class of fabrication strategies for the fast and scalable fabrication of EESDs due to several inherent advantages. Firstly, most printing instruments are inexpensive and can operate in ambient surroundings, enabling EESDs with diverse form factors easily printed in large scale. In addition, printed power sources can be readily self-integrated to tailor output currents and voltages and be seamlessly integrated with other printed electronics into one system. Moreover, these printing technologies are a class of commercially available techniques with board equipment basis, which can directly bridge the gap between laboratory and industry for the scalable production of EESDs [36, 54–58].

Based on this, this review will provide an overview of the recent advancements in printable EESDs for both batteries and supercapacitors and discuss the characteristics, general design principles and suitable applications of different printing technologies in terms of performance and form factor. In addition, this review will present corresponding challenges and propose future research directions.

2 Fabrication and Performance of Printed EESDs

Printing technologies possess a long history and are widely used in the production of books, newspapers, magazines and plastic packaging through the printing of ink involving pigment on substrate due to their simple, effective and scalable operational process [59]. In recent years, the rapid development of functional materials has also led to the significant

expansion of printing technologies in various application fields, and currently, these technologies can be used to fabricate various functional devices (e.g., optics, chemical sensors, transistors, EESDs) [60–64] through the use of functional materials as pigments to prepare printable ink.

In principle, EESDs can be classified into batteries and SCs, both of which possess similar components including current collectors, electrodes, electrolytes and separators but with different energy storage mechanisms [8, 65]. In general, batteries store energy through reversible bulk-phase redox reactions (insertion, conversion and alloy types) and exhibit high energy density and low charge–discharge rate [23, 66–68], whereas SCs store charge through the rapid adsorption and desorption of electrolyte ions or Faradaic reactions at the surface or the near-surface between electrodes and electrolytes and offer high power density, long cycle life but relatively low energy density [2, 35, 69, 70]. As for conventional EESDs, these are commonly assembled in a sandwich structure through the consecutive layer-by-layer (LBL) stacking of a cathode current collector, a cathode, a separator, an anode and an anode current collector followed by the injection of an electrolyte and packaging [71, 72]. And with the recent emergence of flexible and wearable electronics, planar EESDs with cathodes and anodes arranged on a single substrate and separated by empty interspacing have attracted increasing attention due to their favorable mechanical flexibility and robustness through the minimization of interfacial delamination. Here, due to the advantages of high-throughput film preparation and shape customization, printing techniques are regarded as promising strategies for the fabrication of these EESDs, especially towards future application as the power source of smart and wearable electronics requiring diversified form factors [36, 54].

Printed EESDs are usually referred to as batteries and SCs in which at least one component (e.g., current collectors, electrodes, electrolytes, separators) is fabricated through printing [73]. In general, the first step in the fabrication of printed EESDs is the selection of an appropriate printing technique based on application requirements because significant differences exist between different printing processes, including printing resolution, printing speed, printed film thickness, patterning methods and substrate adaptability. The subsequent step is the preparation of component ink with matched rheology and viscosity based on the selected printing strategy because different printing techniques possess different requirements for ink in which suitable rheology and viscosity are vital for smooth printing. For example, high apparent viscosity and shear-thinning inks are desired in screen printing and 3D printing methods and can guarantee the smooth delivery of inks through meshes or nozzles as well as the rapid solidification of the inks following deposition on substrates. Alternatively, low-viscosity inks are desirable in inkjet printing and spray coating methods

to allow for full nebulization. Based on this, comprehensive considerations of device geometry, component ink rheological property, printing technique and cell performance are vital for the successful fabrication of high-performance printed EESDs with desired form factors [36]. Table 1 compares the merits and shortcomings of different printing techniques and summarizes the respective characteristics of various printing methods.

Thus far, great efforts have been devoted to the development of printable EESDs with great progress being achieved in terms of printing strategies, device configurations (e.g., stacked and planar geometries), diverse battery and SC systems [e.g., lithium-ion batteries (LIBs), Zn–Ag batteries, electric double-layer capacitors, pseudocapacitors] and functionalities (e.g., flexibility, stretchability, miniaturization, integration) (Fig. 1) [64, 74–80]. Based on this, the following sections will focus on the recent advancements of printed EESDs based on different printing techniques.

2.1 Spray Coating

Spray coating is a printing technique that makes use of an airbrush to deposit highly atomized component dispersions induced by high-pressure air onto target substrates to form patterned films with the assistance of designable shadow masks [85]. In general, low vapor-pressure solvents and heated substrates are preferred in the spray coating process to allow for the quick evaporation of solvents and the formation of component films, which are highly beneficial for consecutive LBL printing [86]. In addition, spray coating possesses low requirements in terms of ink rheology, thus allowing for excellent process flexibility and maximum

component selection. Moreover, spray coating can allow for film preparation on non-flat substrates due to the non-contact printing nature. Despite these features however, spray printing also suffers from time consumption and low printing resolution and is unsuitable for the scalable production of EESDs, especially with thick electrode films.

As an example of spray printing, Singh et al. [64] addressed the rigid design principles of conventional EESDs (Fig. 2a) by fabricating fully printed LIBs through the sequential spray coating of carbon nanotubes (CNTs), LiCoO₂ (LCO), Kynarflex, poly(methylmethacrylate), Li₄Ti₅O₁₂ (LTO) and conductive Cu dispersions as the cathode current collector, the cathode, the polymer separator, the anode and the anode current collector, respectively (Fig. 2b), on various substrates of stainless steel, glass, polymer sheets and even curved ceramics mug. As a result, the printed LIB exhibited favorable electrochemical performances with a specific capacity of ~120 mAh g⁻¹ (Fig. 2c) and was able to be readily integrated with energy harvesters such as solar cells, thus demonstrating the exceptional applicability of spray coating and the great potential of printed EESDs in the construction of integrated standalone power sources. Spray coating is also promising in the preparation of functionalized components in EESDs such as the interlayers of Li–S batteries. For example, Niu et al. [87] used an electrostatic spray coating technique to coat a cathode with a multifunctional polysulfide blocking layer (MPBL) composed of nanosized carbon black and poly(3,4-ethylenedioxythiophene)/poly(styrenesulfonate) (PEDOT:PSS, PH1000) to restrain polysulfide shuttling effects (Fig. 2d) in which nanosized carbon black-PEDOT:PSS composite ink was immediately aerosolized and charged under a high voltage of 21 kV once

Table 1 Comparison of different printing techniques

Printing type	Pre-pattern	Resolution	Thickness (μm)	Substrate	Printing speed	Instrument cost	Ink properties	On-contact
Spray printing	Yes	Low	1–10	Uneven	Slow	Cheap	Good dispersion, low vapor-pressure solvent	No
Inkjet printing	No	High	0.5–3	Uneven	Rapid	Medium	Low viscosity, long-term stability, small particle-size	No
Screen printing	Yes	Medium	5–200	Flat	Medium	Cheap	High viscosity, shear-thinning	Yes
3D printing	No	Medium	10–200	Uneven	Slow	Expensive	Shear-thinning, low solvent content	No
Gravure printing	Yes	Low	1–3	Flat	Medium	Expensive	Low viscosity, wettability to substrate	Yes
Flexographic printing	Yes	Low	1–3	Flat	Rapid	Expensive	Low viscosity	Yes
Transfer (stamp) printing	Yes	Low	0.5–5	Flat	Slow	Cheap	High content, medium viscosity	Yes
Pen writing	No	Low	0.5–10	Uneven	Slow	Cheap	Good dispersion, low viscosity	Yes

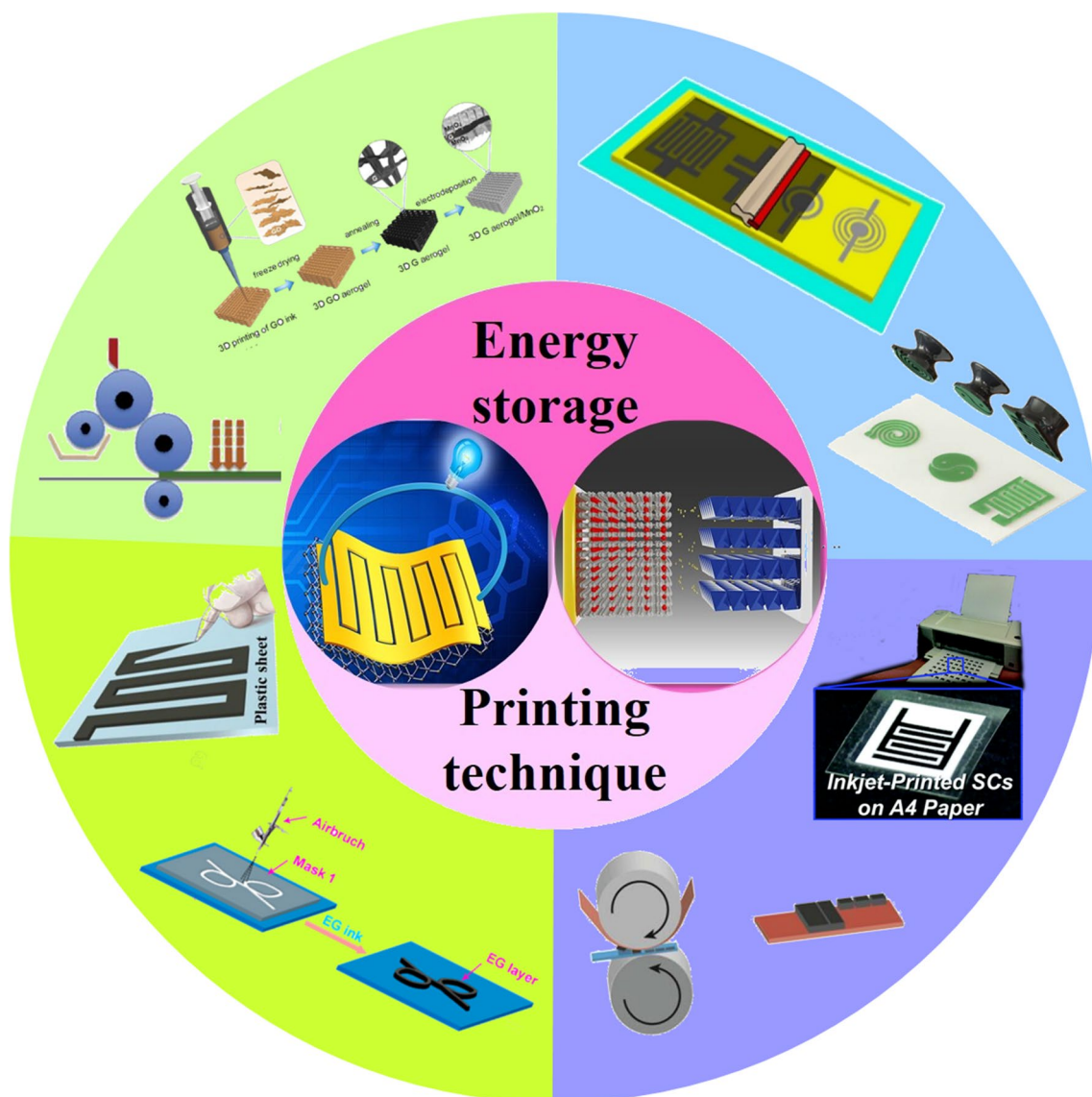


Fig. 1 Overview of various printing techniques for the fabrication of printable EESDs. Reprinted with permission from Refs. [80, 81]. Copyright 2014 and 2019 Elsevier. Reprinted with permission from Refs. [82–84]. Copyright 2014, 2015 and 2018 John Wiley and Sons,

Inc. Reprinted with permission from Refs. [75, 79]. Copyright 2016 and 2019 The Royal Society of Chemistry. Reprinted with permission from Ref. [76]. Copyright 2017 American Chemical Society

ejected from the printing nozzle to allow for the uniform deposition of an ultrathin film onto the cathode due to electrostatic repulsion between the aerosolized small droplets. Here, the synergistic combination of physical adsorption from carbon black, chemical confinement from PEDOT:PSS and fast ion diffusion in the highly conductive and ultrathin MPBL layer together reportedly led to enhanced capacities and better cycling stability (Fig. 2e).

Similar to fully printed LIBs, Wang et al. [86] also developed a consecutive spray coating strategy for the fabrication of an SC utilizing a CNT–polyaniline (PANI) electrode, a cellulose nanofiber (CNF) separator and poly(vinyl alcohol)/

H_2SO_4 (PVA/ H_2SO_4) electrolyte inks on different substrates. However, the volumetric capacitance of this resulting device was unsatisfactory as limited by the thick CNF separator ($\sim 10 \mu\text{m}$). To overcome this issue, Zheng et al. [74] recently fabricated planar stacked microsupercapacitors (MSCs) by spray-coating two types of graphene including high-quality electrochemically exfoliated graphene (EG) as the electrodes and nanosized graphene oxide (GO) as the separator in a sandwich-like layer-stacked structure on one substrate. Here, an ultrathin separator with a thickness of only $\sim 2 \mu\text{m}$ was obtained from the atomically thin nanosized GO nanosheets, allowing the resulting sandwich-like planar MSCs to exhibit

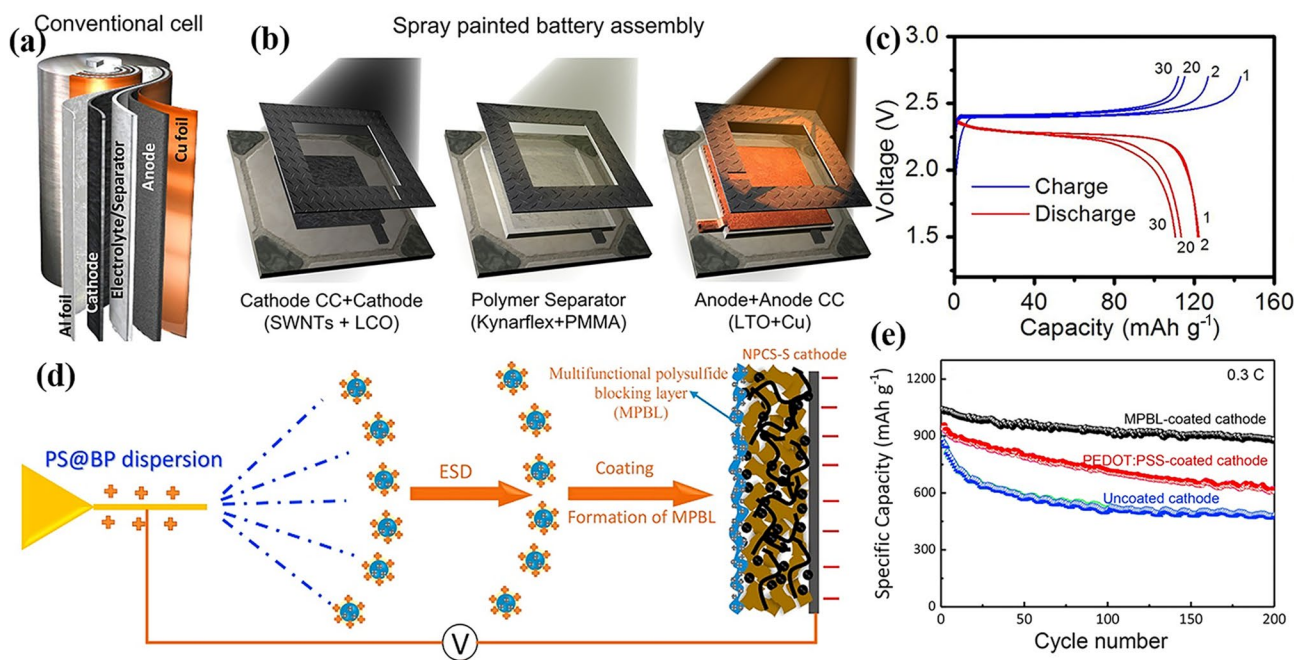


Fig. 2 Battery fabrication through spray coating. **a** Simplified view of a conventional LIB. **b** Direct fabrication of LIBs through the sequential spraying of multiple component inks. **c** Galvanostatic charge and discharge (GCD) profiles for the 1st, the 2nd, the 20th and the 30th cycles of the spray printed LTO/LCO LIB. Reprinted with permis-

sion from Ref. [64]. Copyright 2012 Nature Publishing Group. **d** Fabrication schematic of an MPBL coated electrode through electrostatic spray coating. **e** Cycle performances of MPBL and PEDOT:PSS-coated S cathodes and an uncoated S cathode at 0.3 C. Reprinted with permission from Ref. [87]. Copyright 2016 Elsevier

a high volumetric capacitance of 10.6 F cm^{-3} and an energy density of 0.98 mWh cm^{-3} . To further enhance energy density, asymmetric MSCs were also fabricated through the LBL spray coating of 2D MnO_2 nanosheets/PEDOT:PSS as the positive electrode, 2D boron nitride (BN) nanosheets as the separator and EG as the negative electrode [88]. And as a result of an extended voltage window of 1.8 V, the as-prepared asymmetric MSCs displayed an improved energy density of 8.6 mWh cm^{-3} . Wu et al. [89] also fabricated ultrathin sandwich-like MSCs through the spray coating of an solution-processed EG/PEDOT:PSS film onto an ultrathin Au-coated polyethylene terephthalate (PET) substrate and reported an ultrahigh rate up to 2000 V s^{-1} , a power density of 4386 W cm^{-3} and an outstanding alternating current line-filtering performance with a low resistor–capacitor time constant of less than 1 ms, thus possessing great potential to replace bulky aluminum electrolytic capacitors in integrated circuits.

Aside from stacked geometry, spray coating is also widely used for the fabrication of in-plane SCs. For example, Liu et al. [90] fabricated in-plane MSCs on paper and PET substrates through the use of shadow interdigital masks by spray-coating a hybrid ink composed of EG and PEDOT:PSS (Fig. 3a) and reported that the resulting MSCs offered an areal capacitance of 5.4 mF cm^{-2} and remarkable flexibility. Using spray coating, Shi et al. [85] also fabricated a series

of tandem planar MSCs including highly integrated MSCs based on EG electrodes, high-capacitance MSCs based on PANI electrodes, and high-voltage asymmetric MSCs based on a MnO_2 -PH1000 positive electrode and an EG negative electrode with linear geometry. Especially, the successful demonstration of integrated asymmetric MSCs indicates the remarkable applicability of spray coating techniques in the fabrication of other EESDs such as LIBs with planar structures (Fig. 3b, c).

2.2 Inkjet Printing

Inkjet printing is a high-resolution digital printing technique that utilizes thermoelectric or piezoelectric elements to eject ink droplets onto target substrates. Inkjet printing allows for the direct formation of desired shapes through control from a computer without the need for pre-patterned customized masks [73]. However, multiple ink characteristics including low viscosity, low surface tension, favorable wettability to micronozzles and long-term stability are generally required for inkjet printing to avoid micronozzle clogging and ensure smooth printing processes [36, 54]. In view of this, nanomaterials are highly promising for ink preparation due to their relatively small size, which can efficiently prevent nozzle clogging. Furthermore, surfactants are commonly needed in the preparation of inkjet-printed inks to

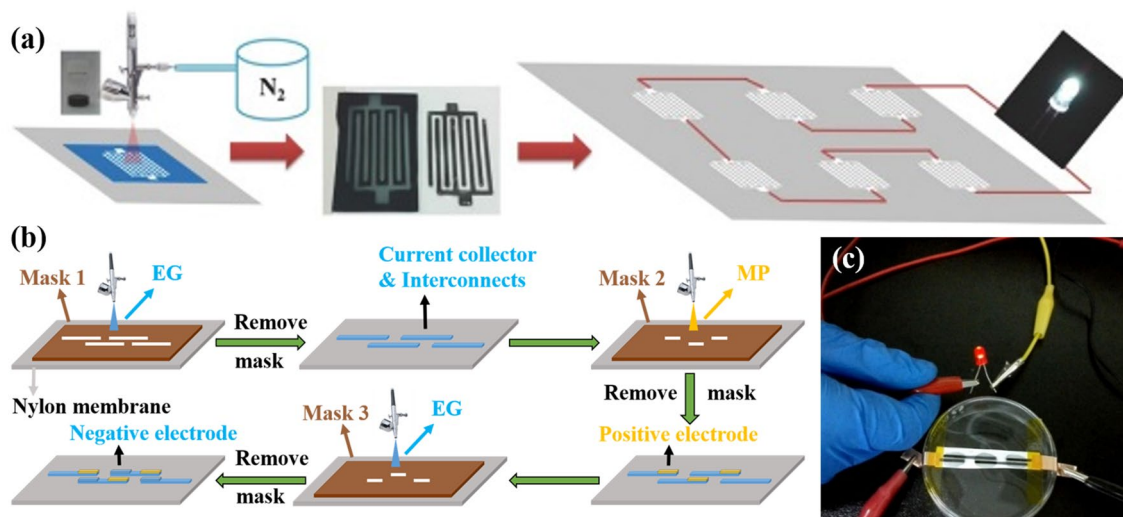


Fig. 3 Fabrication of SCs through spray coating. **a** Schematic of a mask-assisted spray coating method for the direct printing of single and arrayed MSCs. Reprinted with permission from Ref. [90]. Copyright 2016 John Wiley and Sons, Inc. **b** Device fabrication

of asymmetric MSCs based on EG as the negative electrode and $\text{MnO}_2\text{-PH1000}$ as the positive electrode. **c** Photograph of asymmetric MSCs powering a light-emitting diode (LED). Reprinted with permission from Ref. [85]. Copyright 2017 John Wiley and Sons, Inc.

enhance the dispersity of components and modify the viscosity of inks. Despite these requirements, inkjet printing can achieve high resolutions and therefore has been widely applied to fabricate various transistors and sensors [91, 92], thus providing enormous opportunities for the integration of EESDs and other electronics. However, low areal energy densities derived from thin printed films (thickness $\sim 2 \mu\text{m}$) limit the application of inkjet-printed EESDs in low energy consumption situations [54].

Surfactants or binders are usually necessary components for high-dispersity and high-stability inkjet printing inks. To study the effects of different binders, Delannoy et al. [93] prepared a series of LiFePO_4 (LFP)-based aqueous inks with different binders including carboxymethyl cellulose (CMC), isooctyl phenyl ether of polyoxyethylene and polyacrylic-*co*-maleic acid for inkjet printing and carried out corresponding rheological characterizations to find that inkjet-printed electrodes derived from optimized polyacrylic-*co*-maleic acid-based ink can provide a high capacity of 70 mAh g^{-1} at an ultrahigh rate of 90 C. In another example, Zhao et al. [94] inkjet-printed a SnO_2 film anode using CH10B and CH12B as surfactants to stabilize polar SnO_2 nanoparticles and non-polar acetylene black particles, respectively, and reported that the prepared anode film in rechargeable LIBs can exhibit a high initial discharge capacity of 812.7 mAh g^{-1} . Despite these examples demonstrating the importance of surfactants and binders, the addition of inactive and non-conductive surfactants or polymer binders in inks for inkjet-printed EESDs will result in decreased performances. In this regard, Lawes et al. [95] prepared a Si nanoparticle (SiNP)-based ink with highly conductive PEDOT:PSS as a polymer binder to

successfully fabricate its pattern and electrode film through inkjet printing on copper foils (Fig. 4a–c) and reported that as compared with other binders of polyvinylpyrrolidone, CMC and Na alginate (Fig. 4c), PEDOT:PSS provided additional conductive pathways when the SiNPs disconnected from the carbon black network during charge and discharge processes (Fig. 4e). More importantly, the reversible deformation of the PEDOT:PSS binder allowed it to sufficiently stretch and contract with SiNPs, thereby accommodating the large volume change of the SiNPs during cycling (Fig. 4e). As a result, the SiNPs with the PEDOT:PSS binder exhibited remarkable stability in 1000 cycles of limited depth-of-discharge (1000 mAh g^{-1}) measurements (Fig. 4d) and demonstrated the importance of exploiting highly conductive binders for ink preparation.

Although inkjet printing is usually unsuitable for the fabrication of common thick electrode EESDs because of the low thickness of printed films, it still holds great potential in the fabrication of transparent devices [96, 97]. For example, Cheng et al. [97] constructed a highly transparent film through inkjet printing a PEDOT:PSS/Ag grid hybrid ink in which the combination of PEDOT:PSS and Ag grids can effectively compensate for respective demerits. Here, Ag grids can provide additional conductive paths and act as current collectors for PEDOT:PSS, whereas PEDOT:PSS layers can effectively enhance the anti-oxidation ability of Ag grids. And as a result, the inkjet-printed hybrid film can exhibit remarkable optoelectronic performances with a high light transmittance of 89%, a low sheet resistance of $12 \Omega \text{ sq}^{-1}$, and significantly improved stability. Further, the highly transparent SCs with esthetically pleasing appearance

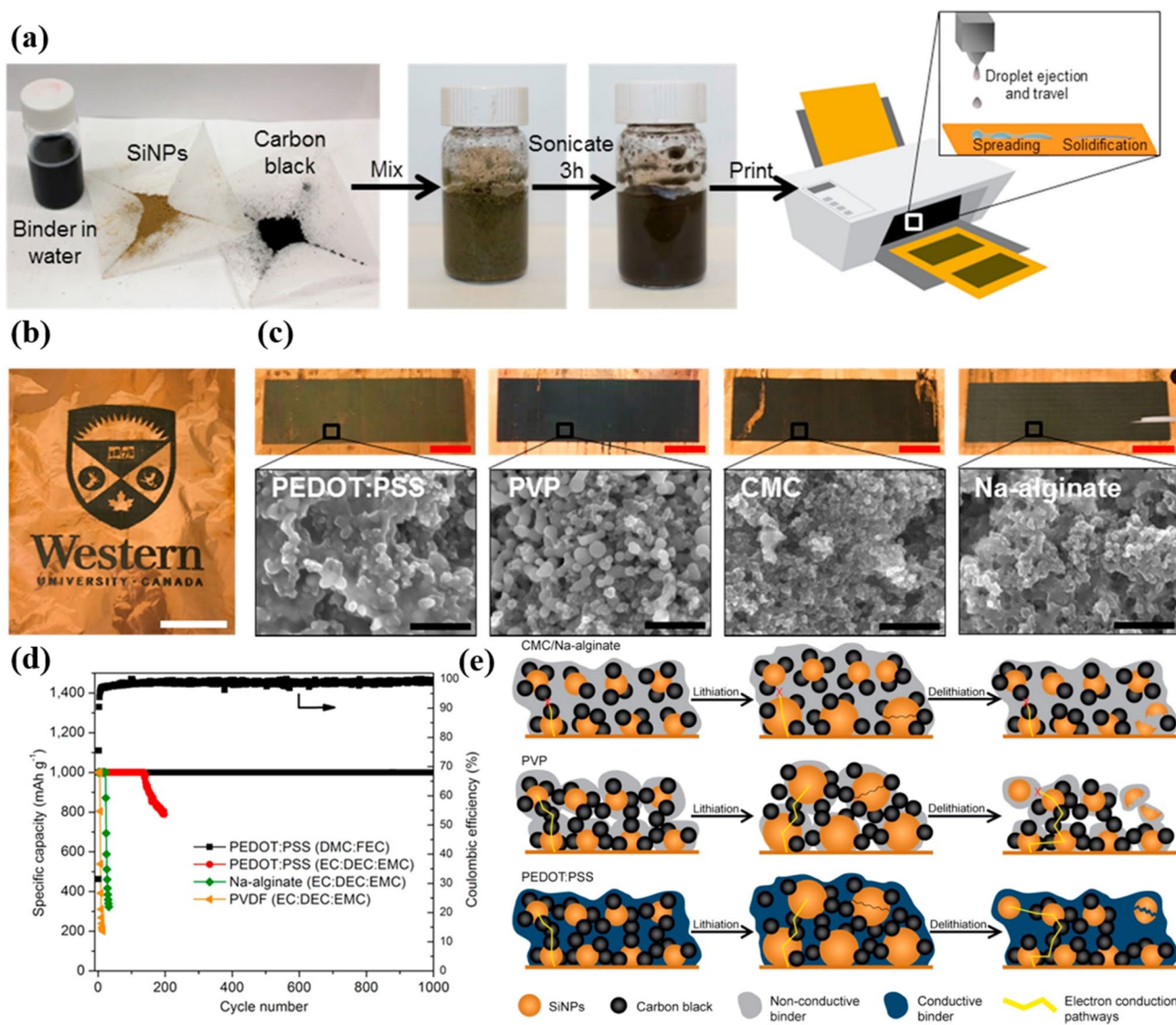


Fig. 4 Fabrication of batteries through inkjet printing. **a** Procedure of inkjet-printed silicon-based anodes. **b** Photograph of an inkjet-printed Western University logo by using SiNP ink. **c** Photographs and SEM images of inkjet-printed SiNP anode films on copper foil with different binders. Red, white and black scale bars represent 3 cm, 5 cm and

500 nm, respectively. **d** Limited depth-of-discharge tests performed at a capacity cutoff of 1000 mAh g⁻¹. **e** Schematic of a proposed mechanism explaining the performance of anodes prepared by using different binders. Reprinted with permission from Ref. [95]. Copyright 2017 Elsevier

were assembled by using the inkjet-printed electrodes and exhibited a high areal capacitance of 1.13 mF cm⁻².

Actually, inkjet printing is more suitable for the fabrication of planar EESDs due to the favorable high-resolution patterning ability [75, 98–101]. Here, the key to realize high-resolution inkjet printing is to balance the surface tension between ejected droplets and target substrates because unmatched surface tensions usually lead to the random spreading of ink droplets and resolution degradation on wetting substrates or the formation of coffee rings and the poor adhesion of printed films on non-wetting substrates. In order to simultaneously optimize printing resolution and

adhesion, the incorporation of suitable polymer additives into inks to adjust surface tension is a common strategy, but it would result in the inferior performance of printable EESDs [102]. To resolve this, Choi et al. [75] inkjet printed a CNF primer layer on conventional wetting (A4 paper) and non-wetting (PET) substrates to prevent the random spreading of ink droplets, the formation of coffee rings and the poor adhesion. And as a result, the CNF-enhanced paper and PET combined the advantages of wetting and non-wetting substrates to achieve high-resolution printing on conventional substrates. Using this approach, they designed and fabricated an all-inkjet-printed solid-state SCs based on

activated carbon (AC)/CNTs electrodes and an ultraviolet (UV)-curable 1-butyl-3-methylimidazolium tetrafluoroborate (BMIMBF₄)-based electrolyte (Fig. 5a, b) and reported enhanced performances. It is worth mentioning that the principle of surface tension balance between the inks and substrates is similar for other printing strategies. However, the Ag nanowires were still required to enhance electrical conductivity in this study, thus limiting its practical application. More recently, Ti₃C₂T_x MXene has been regarded as a competitive electrode material candidate for SCs, due to its high volumetric capacitance and metallic conductivity [16, 103]. More importantly, pure MXene possesses remarkable dispersibility in water and some organic solvents without the need for any surfactants, which cannot be achieved for most conductive nanomaterials such as graphene or CNTs [101, 104]. Based on this, Zhang et al. [105] developed high-concentration (12.5 mg mL⁻¹), additive-free organic MXene inks for inkjet printing (Fig. 5c). Through the careful

selection of Al₂O₃-coated PET to guarantee the matching of surface tensions between MXene droplets and substrates (Fig. 5d), high-resolution (an ~80 μm width and a ~50 μm gap) interdigital MXene patterns were successfully achieved (Fig. 5e, f). Moreover, the sheet resistance and current–voltage results of the prepared MXene lines with different printing times demonstrated outstanding homogeneity and reproducibility (Fig. 5g, h) and that the final printed MSCs presented an areal capacitance of 12 mF cm⁻² and favorable rate performances.

Aside from symmetric SCs, inkjet printing can also be used for the fabrication of high-energy asymmetric SCs. For example, Sundriyal et al. [76] prepared asymmetric SCs through the inkjet printing of a reduced GO (rGO)-MnO₂ hybrid positive electrode along with an AC negative electrode and a PVA-LiCl gel electrolyte and reported that the resulting SCs possessed a wide voltage window of 2 V and an enhanced energy density of 22 mWh cm⁻³ as well

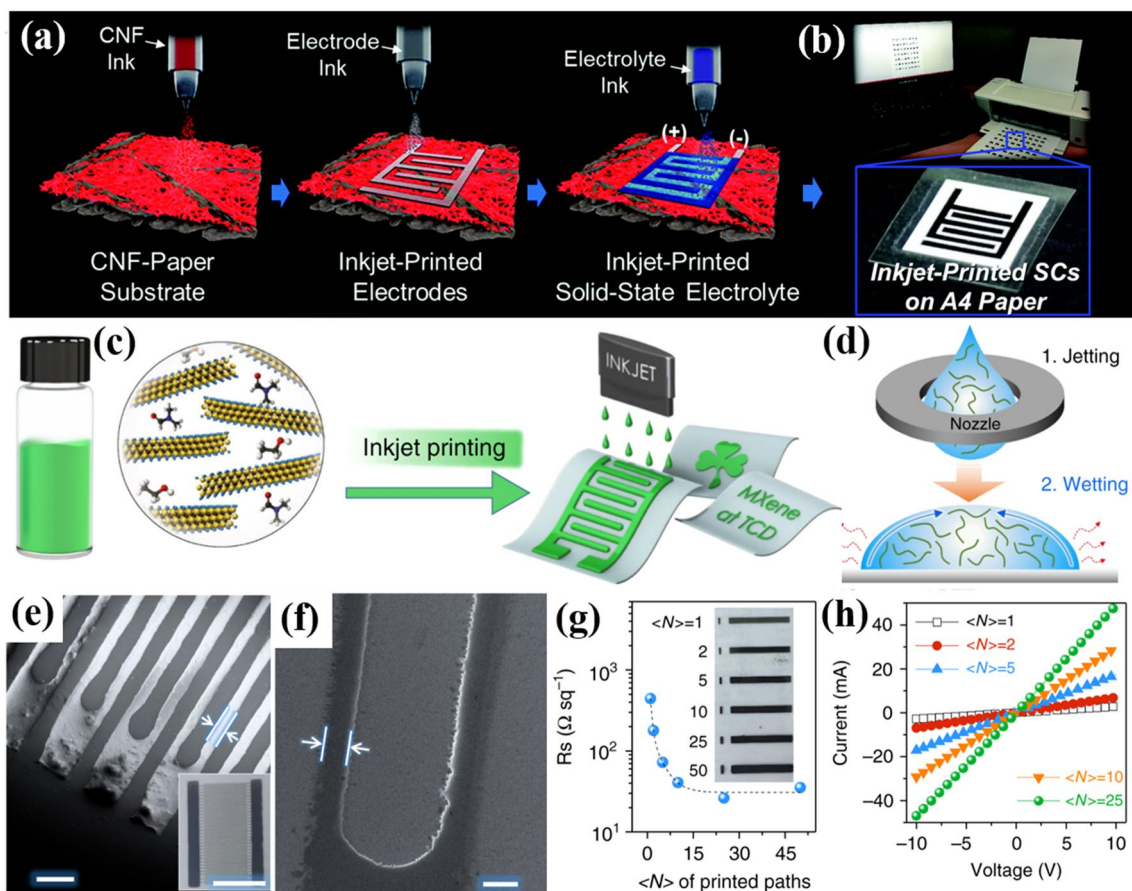


Fig. 5 Fabrication of SCs through inkjet printing. **a** Schematic of the fabrication of all-inkjet-printed SCs. **b** Photographs of an inkjet printer and inkjet-printed SCs. Reprinted with permission from Ref. [75]. Copyright 2016 The Royal Society of Chemistry. **c** Schematics of organic MXene ink and the inkjet printing process. **d** Schematic of the wetting of inkjet-printed MXene ink onto an Al₂O₃ coated

substrate. **e, f** SEM images of inkjet-printed MSCs by using MXene ink with *e* N-methyl-2-pyrrolidone (NMP) and *f* ethanol as solvents. Scale bar is 200 μm in **e, f** and 1 cm in the inset of **e**. **g** Sheet resistance as a function of inkjet-printed paths. **h** I–V curves of MXene lines with different inkjet-printed paths. Reprinted with permission from Ref. [105]. Copyright 2019 Nature Publishing Group

as favorable flexibility and aesthetic properties. In addition to nanomaterials, inkjet-printed planar MSCs based on commercially available electrode materials have also been demonstrated by Brunet et al. [98] in which a stable ink was prepared by mixing an AC electrode with a polytetrafluoroethylene binder and a Triton X100 surfactant in ethylene glycol followed by inkjet printing onto interdigital Au current collectors. The obtained MSCs tested in an electrolyte of 1 M Et_4NBF_4 in propylene carbonate (PC) could operate stably at a wide voltage window of 2.5 V and show a device capacitance of 2.1 mF cm^{-2} , demonstrating the great potential of inkjet printing in the construction of commercial EESDs.

2.3 Screen Printing

Screen printing (or stencil printing) is an industrially applicable printing technique involving the use of a squeegee to drag component ink through screens with meshes (or stencils) to deposit predesigned patterns onto substrates [36, 54] in which screen-printed films are $\sim 10^1 \mu\text{m}$ thick, approaching the typical thickness of conventional batteries [36]. And because screen printing is a simple process that is also inexpensive, it is widely used in various fields such as the printing of texts and patterns on fabrics [54]. Despite this, the biggest challenge of screen printing is the preparation of component inks, which need to be highly viscous in static states but also possess shear-thinning behaviors in order to smoothly go through screens and immediately solidify to maintain predesigned patterns. In addition, screen printing possesses limited process flexibility and printing resolution as compared with inkjet printing due to the pre-patterned step in the preparation of screens or stencils.

Screen printing is widely used in cloth manufacture; therefore, it is naturally regarded as a promising mass-production technique to fabricate wearable EESDs. For example, Jost et al. [106] developed screen-printed textile SCs based on knitted carbon fiber and AC ink and obtained a high areal capacitance of 0.51 F cm^{-2} . However, the obvious performance degradation was observed in bending states. To improve this, Abdelkader et al. [107] also fabricated solid-state SCs by screen printing GO ink onto a textile followed by an in situ electrochemical reduction step to convert it into rGO electrodes. As a result, the obtained device provided favorable mechanical flexibility due to strong interaction between the printed electrodes and the textile substrate. Nevertheless, it should be further simplified since an extra reduction process is still required to convert GO to conductive rGO, increasing the complexity of device manufacturing. Alternatively, Liu et al. [108] prepared flexible MSCs using an LBL screen printing process in which Ag paste was used as the current collectors and N-doped rGO was used as the microelectrodes. The as-made MSCs showed areal

capacitance of 3.4 mF cm^{-2} and excellent cycling stability with 98.4% retention after 2000 cycles. In another example, Liu et al. [109] fabricated all-printed asymmetric MSCs through the multiple screen printing of Ag current collector ink, AC-waterborne resin anode ink, Ag@polypyrrole@ MnO_2 -waterborne (Ag@ppy@ MnO_2) resin cathode ink and Na_2SO_4 -PVA electrolyte ink on a stretchable textile substrate (Fig. 6a). Here, these researchers reported that the obtained asymmetric SCs not only exhibited an excellent areal capacitance of 95.3 mF cm^{-2} and remarkable stability of 98.7% capacitance retention after 10000 cycles, but also possessed favorable mechanical properties with 86.2% capacitance retention under 40% stretching strain, indicative of the potential of screen printing in the fabrication of wearable EESDs. To further improve specific capacitance, Li et al. [110] also incorporated $\text{Ru}(\text{OH})_3$ nanoparticles into a hybrid electrode ink containing Ag nanowires and GO in which the ternary ink not only ensured high viscosity and shear-thinning properties without the need for additional additives, but also simultaneously guaranteed highly conductive electron pathways, excellent rate capabilities and high specific capacitances after the annealing of $\text{Ru}(\text{OH})_3$ and the reduction in GO. And as a result of the elaborated selection of these three materials and their synergistic effects, the resulting MSCs delivered a remarkable volumetric capacitance of 338 F cm^{-3} and an energy density of 18.8 mWh cm^{-3} , higher than most printed SCs [74, 79, 111]. Despite these promising findings however, the simple and rapid fabrication of screen-printed SCs has not been fully achieved. To address this issue, Shi et al. [79] recently developed a graphene-based conductive ink that simultaneously possesses outstanding rheological, electrical and electrochemical properties for screen printing (Fig. 6b, c). Usage of this highly conductive graphene ink as current collectors and microelectrodes can allow for the simple, rapid, cost-effective and scalable fabrication of MSCs on different insulating substrates (e.g., PET, glass, A4 paper) with diverse geometry (e.g., interdigital, parallel strip, concentric circle, circular interdigital), superior aesthetic properties and outstanding flexibility (Fig. 6d–g). More importantly, the fabrication process using this newly developed ink only required several seconds to finish without the need for additional post-treatment steps, thus largely reducing the time and improving the efficiency of fabricating screen-printed MSCs.

In most screen printing processes, the evaporation of solvents is slow. To improve this, Lee et al. [112] developed a UV-assisted screen printing technique for the fabrication of LIBs to avoid the solvent-evaporating process in which through the incorporation of UV-curable ethoxylated trimethylolpropane triacrylate (ETPTA) monomer and 2-hydroxy-2-methyl-1-phenyl-1-propanone (HMPP) as UV initiators in the electrolyte and electrode pastes, the solidification process can be significantly shortened ($\sim 20 \text{ s}$)

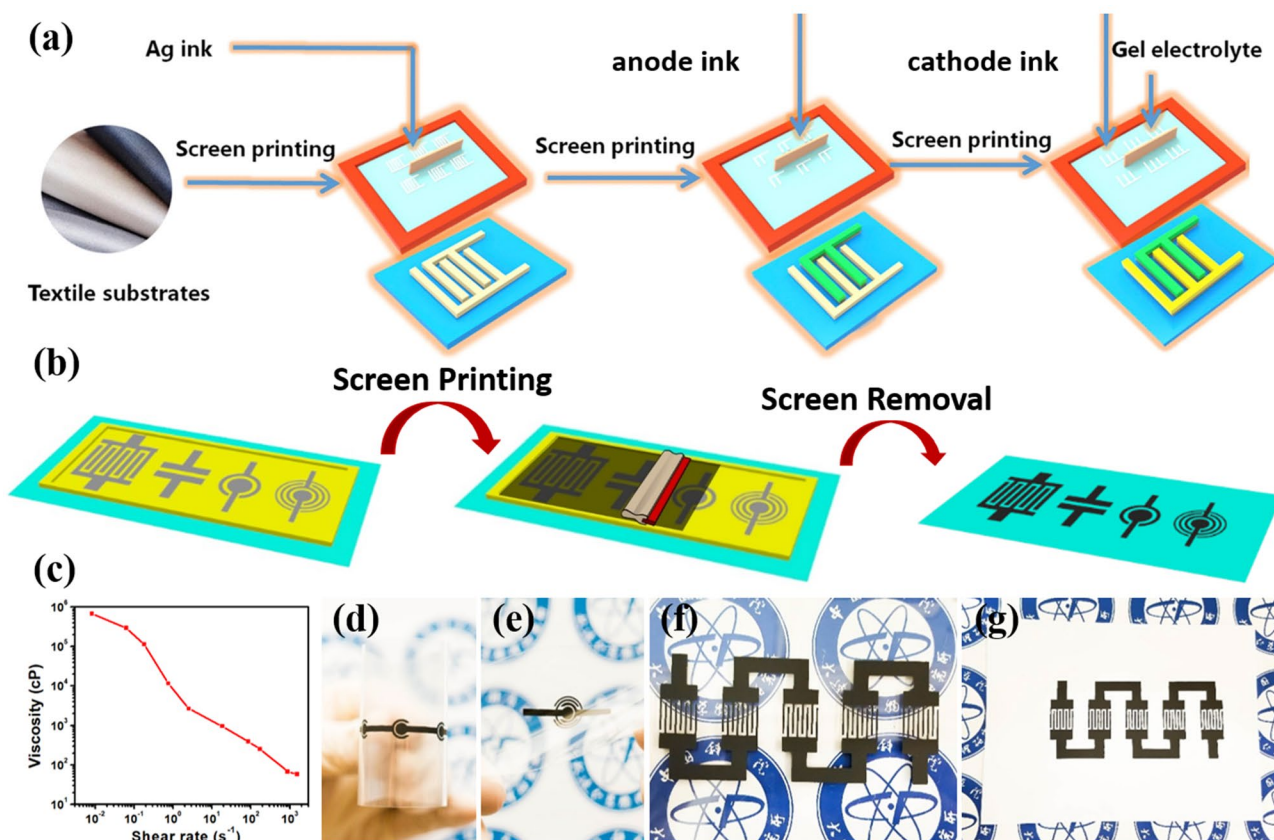


Fig. 6 Fabrication of SCs through screen printing. **a** Fabrication schematic of all-screen-printed asymmetric SCs. Reprinted with permission from Ref. [109]. Copyright 2016 Elsevier. **b** Schematic of the fabrication of screen-printed graphene-based MSCs with diverse planar geometry. **c** Viscosity of graphene-based ink as a function of

the shear rate. Photographs of screen-printed MSCs with **d** concentric circle and **e** circular interdigital shaped geometry on PET substrates. Photographs of interdigital screen-printed MSCs on **f** glass and **g** A4 paper. Reprinted with permission from Ref. [79]. Copyright 2019 The Royal Society of Chemistry

through exposure to UV light after each screen printing step, including LTO anode printing, electrolyte printing and LFP cathode printing, thus greatly improving fabrication efficiency. The resulting printed LIBs exhibited a high capacity of $\sim 160 \text{ mAh g}^{-1}$ (based on LFP mass), which approached the theoretical capacity of LFP. Furthermore, Kim et al. [77] reported that the introduction of poly(vinylidene difluoride-*co*-hexafluoropropylene) (PVDF-HFP) as a linear polymer and the replacement of common carbonate solvents with high boiling point sebaconitrile solvent can allow their resulting screen-printed quasi-solid-state LIBs to deliver impressive safety, flexibility and robustness, in which the LIBs operated stably after a cutting test, 100 bending cycles and even an ignition test (Fig. 7a–f). A similar strategy can also be applied in the screen printing of aqueous batteries. For example, Braam et al. [113] fabricated Zn–Ag₂O batteries by combining screen printing with an UV-polymerizable poly(acrylic acid) separator and reported that the resulting device provided a high capacity of 5.4 mAh cm^{-2} at a discharge rate of 0.5 C. In addition, it is worth mentioning that

the whole process can operate in ambient environments due to the aqueous nature of the system, thereby possessing wide applicability.

2.4 3D Printing

In recent years, 3D printing, also known as additive manufacturing, has drawn increasing attention as a class of efficient, economical and process-flexible fabrication technologies that can be applied to various fields, including microscale electronics, large machineries and chemical biology [114, 115]. These technologies include laminated object manufacturing, selective laser melting (SLM), fused deposition modeling, stereolithography and direct ink writing and have been widely researched. In terms of EESDs, 3D printing is usually referred to the extrusion-based dispenser printing strategy in which component inks go through nozzles driven by pressure and are LBL deposited onto substrates to construct predesigned patterned 3D structures as controlled by a computer [116]. In principle,

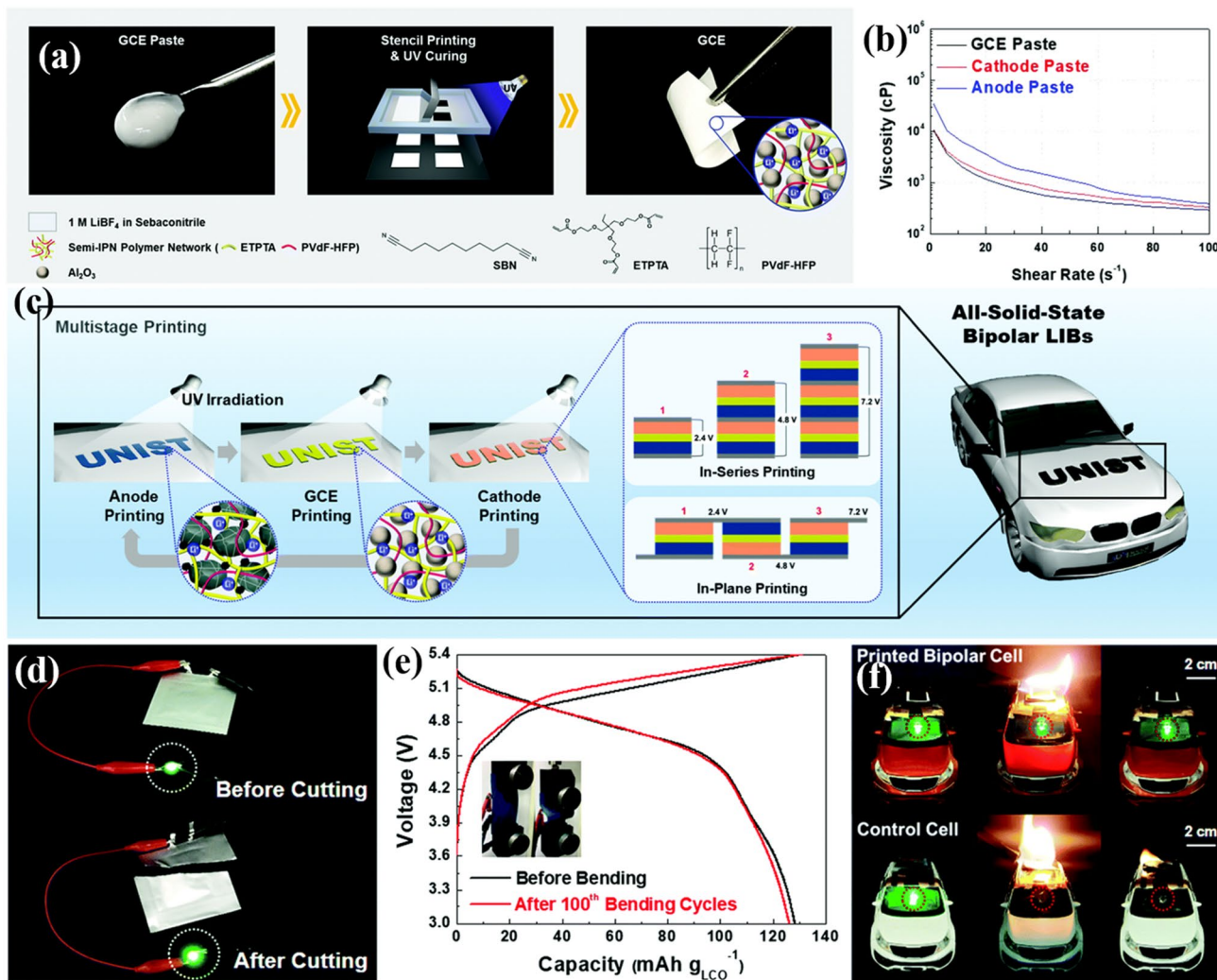


Fig. 7 Fabrication of batteries through screen printing. **a** Schematic of the fabrication of a screen-printed gel composite electrolyte (GCE) along with photographs of the GCE and its major components. **b** Viscosities of GCE, cathode and anode inks as a function of shear rate. **c** Schematic of the fabrication of flexible and shape-versatile batteries through UV-assisted multi-step screen printing. **d** Photographs show-

ing the safety and robustness of printed batteries in a cutting test. **e** GCD profiles of printed 2 stacked batteries in series before/after 100 bending cycles. **f** Non-flammability testing of the printed batteries and control batteries. Reprinted with permission from Ref. [77]. Copyright 2018 The Royal Society of Chemistry

the ink used in 3D printing should possess favorable dispersity, high viscosity and shear-thinning properties to prevent clogging nozzles and enable quick solidification after deposition on target substrates [36, 54, 55]. However, because of the inactive and insulating properties of most rheological additives, a balance between smooth printing process and good electrochemical performance needs to be considered. In addition, the speed of 3D printing is relatively slow as compared with other printing techniques. Despite this, 3D printing is extremely suitable for the fabrication of EESDs with high mass loading or 3D array electrodes and can readily prepare EESDs on non-flat substrates because of the intrinsic property of non-contact printing, similar to spray coating.

As a typical example, Sun et al. [117] used 3D printing to fabricate LIBs with interdigital geometry (Fig. 8a–c) in which to control ink solidification and enhance adhesion during printing, a novel solvent system with graded volatility was developed. Here, a low boiling point solvent (water) was used to induce partial solidification and high boiling point solvents (ethylene glycol and glycerol) were used to ensure strong bonding between layers. Furthermore, through comprehensive optimizations to the composition, viscosity and solid content of their cathode and anode inks, the as-prepared 3D-printed LIBs with interdigital LTO anodes and LFP cathodes displayed a high capacity of ~ 1.5 mAh cm⁻². Similarly, Fu et al. [118] developed 3D-printed LIBs by using GO to adjust the rheology of LFP and LTO inks as

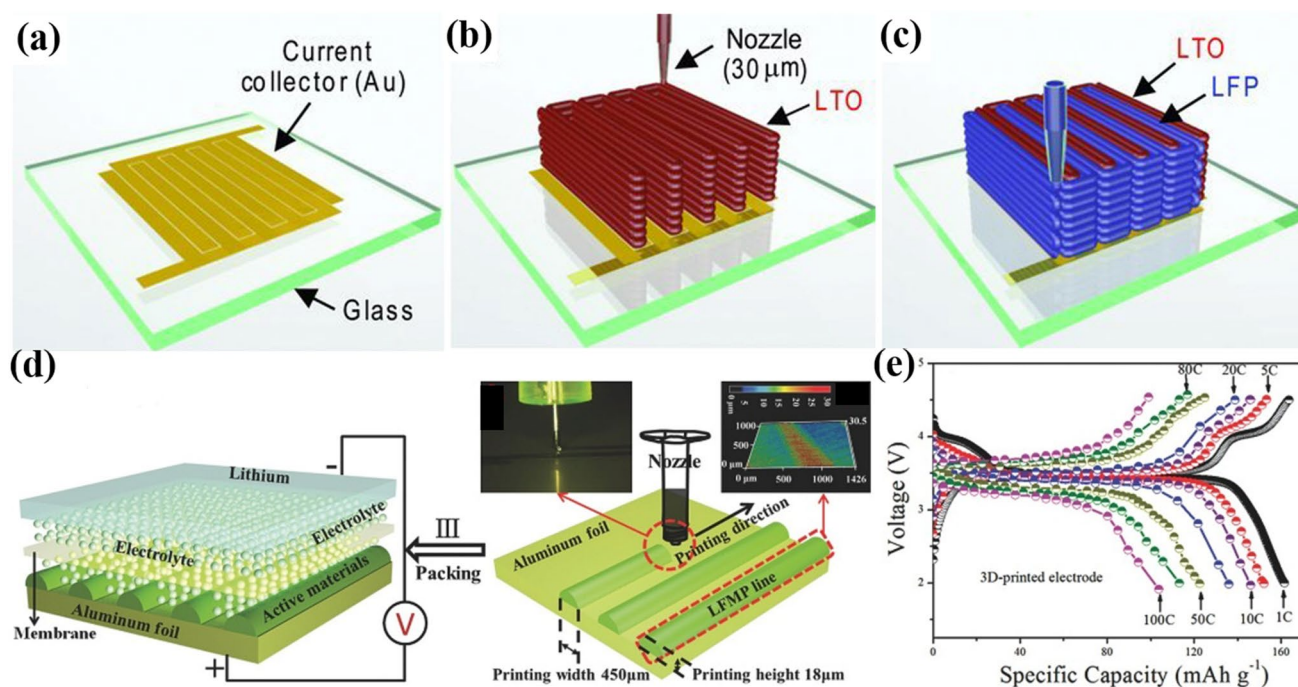


Fig. 8 Fabrication of batteries through 3D printing. **a** Schematic of Au current collectors on a glass substrate. **b**, **c** Fabrication schematic of 3D-printed **b** the LTO anode and **c** the LFP cathode. Reprinted with permission from Ref. [117]. Copyright 2013 John Wiley

and Sons, Inc. **d** Schematic of the assembly of a half-cell based on 3D-printed LFMP electrodes. **e** GCD profiles of 3D-printed electrodes tested at different rates. Reprinted with permission from Ref. [121]. Copyright 2016 John Wiley and Sons, Inc.

inspired by the gel-like behavior and high elastic modulus of high-concentration GO ($\sim 85 \text{ mg mL}^{-1}$) and reported that the addition of highly concentrated GO not only endowed the inks with suitable viscosity and rheology to ensure smooth printing, but also provided excellent conductive pathways after reduction. Moreover, a large number of voids were formed during the removal of gas and the restacking of rGO flakes during thermal annealing, which allowed for the sufficient penetration of electrolytes and contributed to outstanding rate capabilities in which the resulting LFP/rGO and LTO/rGO half-cell exhibited high initial discharge capacities of 164 mAh g^{-1} and 185 mAh g^{-1} that approached respective theoretical capacities. Furthermore, a full cell in this study provided a capacity of $\sim 100 \text{ mAh g}^{-1}$ in charge–discharge tests of ten cycles. Despite this, longer cycling was unavailable to further evaluate performance in this study.

Aside from electrodes, 3D printing can also be used to prepare gel- or solid-state electrolytes. For example, Blake et al. [119] developed a ceramic–polymer electrolyte film with uniform sub-micrometer pores for LIBs through a phase inversion strategy using NMP as a good solvent and glycerol as a weak solvent of PVDF along with nanosized Al_2O_3 as a filler. The resulting electrolyte not only exhibited comparable electrochemical performances to commercial polyolefin separators in half-cell testing with an LFP cathode, but also allowed for direct printing onto composite

electrodes for the construction of corresponding batteries, demonstrating the potential in the completely additively manufactured LIBs. In another example, Lewis et al. [120] developed fully 3D-printed LIBs through sequent multiple printing processes using the polyvinylpyrrolidone (PVP)-stabilized LTO anode and the LFP cathode inks, and UV-curable electrolyte and package inks to eliminate the need for vacuum drying, liquid electrolyte injection, clamping and heat-sealing processes in conventional LIB manufacturing. More importantly, the corresponding LIBs based on the printed thick electrodes (1 mm) exhibited a superior areal capacity of $\sim 15 \text{ mAh cm}^{-2}$, representing the prospect of 3D-printed EESDs in microscale electronic applications that require high energy densities in limited areas.

Apart from the construction of full cells, 3D printing can also assist in the design of electrodes to improve electrochemical reaction kinetics. For example, Hu et al. [121] used 3D printing to construct stereo microelectrodes consisting of multiple parallel $\text{LiMn}_{0.32}\text{Fe}_{0.79}\text{PO}_4\text{@C}$ (LMFP) lines (Fig. 8d) and reported that due to this advanced geometry that is extremely favorable for electrolyte diffusion, the as-prepared LMFP nanocrystal electrode achieved a capacity of $\sim 108 \text{ mAh g}^{-1}$ at an ultrahigh rate of 100 C and a high reversible capacity of 150 mAh g^{-1} at 10 C (Fig. 8e), which were much higher than those of contrastive traditional electrodes. 3D printing can also be applied to other battery

systems as well, including Zn ion batteries, lithium metal batteries, Li–S batteries and Li–O₂ batteries [122–126]. For example, Cao et al. [123] reported the first 3D-printed lithium metal batteries through a two-step strategy involving the 3D printing of a CNF scaffold and a subsequent melted lithium infusion to avoid the difficult process of directly printing lithium metal. The porous CNF scaffold could not only improve ion accessibility, but also decrease current density in lithium anodes and therefore effectively suppress dendrite formation. As a result, a corresponding full cell based on the 3D-printed lithium metal anode and an LFP cathode exhibited a capacity of 80 mAh g⁻¹ at a high rate of 10 C and remarkable stability with 85% capacity retention after 3000 cycles.

In order to maintain the unique characteristics of graphene and analogous 2D materials in functional devices, great efforts have been devoted to the design and assembly of 2D materials in the fabrication of various devices [127–132]. However, high specific capacitances in graphene-based thick electrodes reaching the level in thin-film (~ 10⁰ μm) electrodes remain challenging to achieve for SCs. To overcome this, Zhu et al. [116] proposed a 3D printing method using a homogeneous, highly viscous and thixotropic ink prepared by mixing GO, graphene nanoplates, sodium carbonate and silica fillers to fabricate a millimeter-thick hierarchical graphene aerogel electrode and reported that the resulting 3D-printed electrode displayed a capacitance of 70 F g⁻¹ and exceptional rate capability with 90% capacitance retention from 0.5 to 10 A g⁻¹. Despite these performances, the extended application of this printing method is limited by the complex post-treatment process, which involves the use of highly corrosive HF to etch silicon. To improve this, Jiang et al. [133] developed a facile ion-induced gelation strategy to prepare GO-based printable inks in which aqueous GO dispersions can be converted into printable ink with high viscosity, optimal storage modulus and shear thinning behaviors with the trace addition of Ca²⁺ ions (concentration of 5–10 mM) to ensure a smooth printing process in ambient environments. Owing to the hierarchical porous structure and the high electrical conductivity as well as the trace addition of inactive components, the resulting 3D-printed graphene electrodes delivered an improved capacitance of 213 F g⁻¹ and favorable cycling stability with 90% capacitance retention after 50000 cycles. Alternatively, researchers have also proposed 3D-printed prototype thick electrodes that can significantly enhance the areal capacitance of SCs to levels of ~ 10⁰ and even ~ 10¹ F cm⁻² [80, 134]. For example, Yao et al. [80] incorporated pseudocapacitive MnO₂ nanosheets into rGO aerogels through a combination of 3D printing and electrodeposition (Fig. 9a) and reported that the unique 3D porous

electrode structure was highly conductive and extremely accessible for electrolytes, thus providing efficient electron and ion conduction pathways simultaneously even in the case of thicker electrodes. The resulting 3D electrodes with an ultrahigh MnO₂ loading of 182.2 mg cm⁻² (two orders of magnitude higher than the typical mass loading of conventional electrodes, Fig. 9b) exhibited a recorded areal capacitance of 44.13 F cm⁻², which is at least two orders of magnitude higher than most reported SCs. More importantly, the 3D graphene/MnO₂ electrodes prepared in this study simultaneously achieved high areal, volumetric and gravimetric specific capacitances that circumvented the common trade-off relationship between each property (Fig. 9c–e), thus indicating the great potential of printable EESDs in applications requiring high areal energy.

Aside from stacked structures, planar SCs can also be prepared by means of 3D printing. For example, Rocha et al. [135] fabricated 3D-printed Cu current collectors and rGO electrodes utilizing water-based thermo-responsive inks. However, further optimizations in ink preparation and device geometry were necessary for enhanced electrochemical performance. And similar to graphene, thick MXene-based electrodes with ultrahigh areal capacitances can also be successfully fabricated by using 3D printing [136, 137]. For example, Yu et al. [137] used a melamine formaldehyde templating strategy to fabricate N-doped MXene (MXene-N) and further prepared hybrid inks composed of MXene-N, CNTs, GO and AC for 3D printing without the need for any inactive or insulating additives, resulting in a 3D-printed electrode that exhibited an ultrahigh areal capacitance of 8.2 F cm⁻², which exceeded most MXene-based SCs [53, 138]. Furthermore, Liu et al. [139] also fabricated asymmetric SCs through the 3D printing of GO-PANI positive electrode inks and rGO negative electrode inks onto interdigital Au current collectors, delivering an energy density of 4.83 mWh cm⁻³ [138, 139]. Moreover, it is worth noting that highly conductive PH1000 was used as a viscosity and rheology modifier to provide high electron transfer pathways and capacitances for the obtained SCs. Researchers have also suggested that 3D printing is highly promising in the construction of 3D microelectrode array architectures that can simultaneously possess remarkable electrical conductivity and high aspect ratios for electrolyte ion diffusion to lead to high energy and power densities in EESDs [24]. Based on this, Wallace et al. [140] created 3D array titanium current collectors using an SLM 3D printing strategy followed by the electrodeposition of polypyrroles as active electrode materials. Here, these researchers reported that although the assembled all-solid-state SC with a PVA/H₃PO₄ electrolyte exhibited typical capacitive behaviors, the anticipated high specific capacitance and rate performance were not fully obtained.

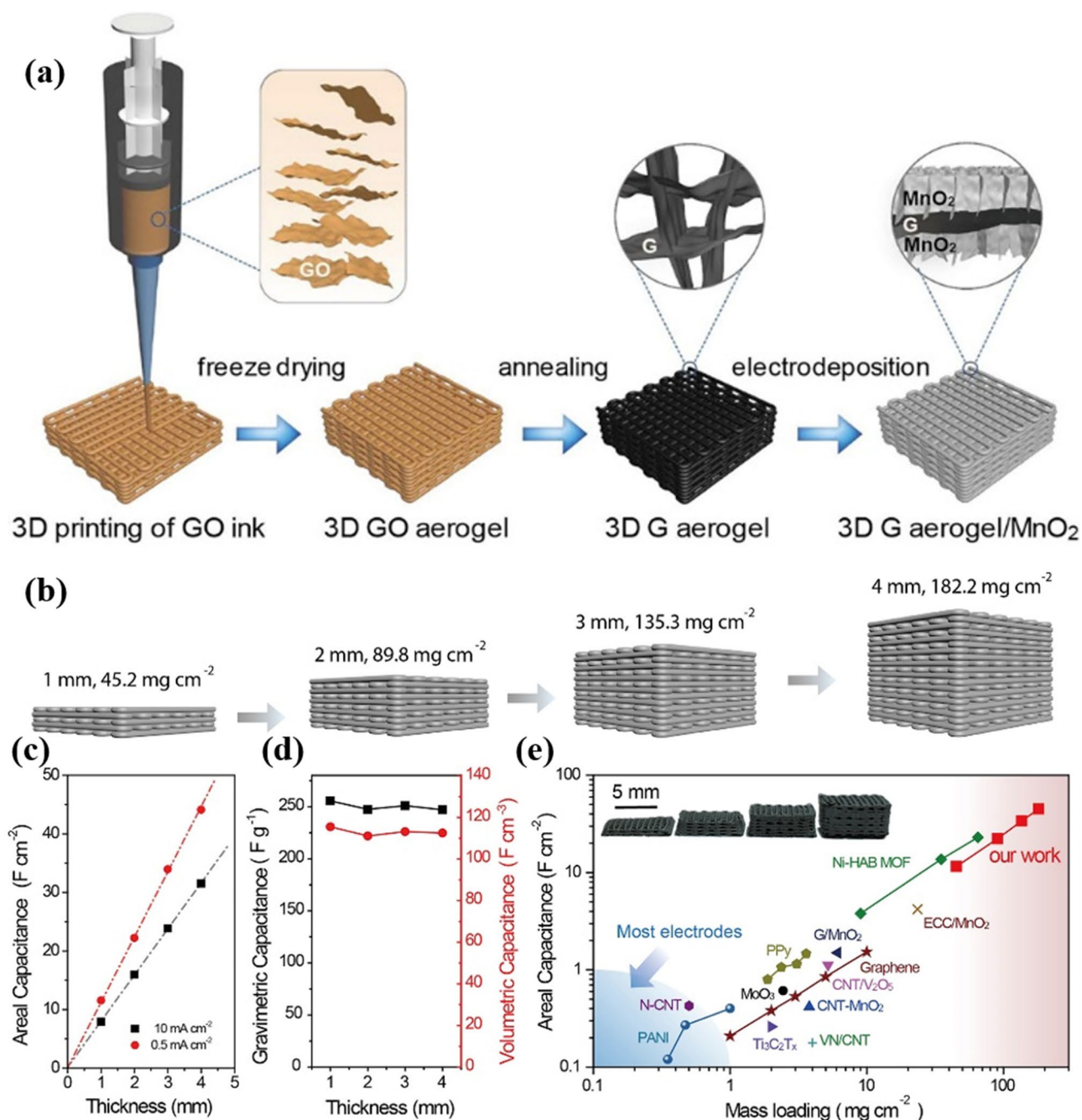


Fig. 9 Fabrication of SCs through 3D printing. **a** Fabrication schematic of 3D-printed graphene aerogel/MnO₂ electrodes. **b** Schematic of graphene/MnO₂ electrodes with different thicknesses and mass loadings of MnO₂. **c** Areal capacitance of 3D-printed electrodes tested at 0.5 and 10 mA cm⁻² as functions of electrode thickness. **d**

Gravimetric and volumetric capacitances as functions of electrode thickness. **e** Plot comparing the areal capacitance of 3D-printed graphene/MnO₂ electrodes with values from previous publications. Reprinted with permission from Ref. [80]. Copyright 2018 Elsevier

2.5 Other Printing Techniques

Other printing strategies have also been developed for the fabrication of EESDs. One example is flexographic printing, which is a fast and inexpensive class of mature and important printing techniques extensively used in the printing of

texts and logos on food packaging [59]. In general, standard flexographic printing instruments contain multiple cylinders and the printing process is carried out through sequential transition steps between the cylinders. With the usual thickness of flexographic-printed films being ~3 μm, it is less than the characteristic electrode thickness of common

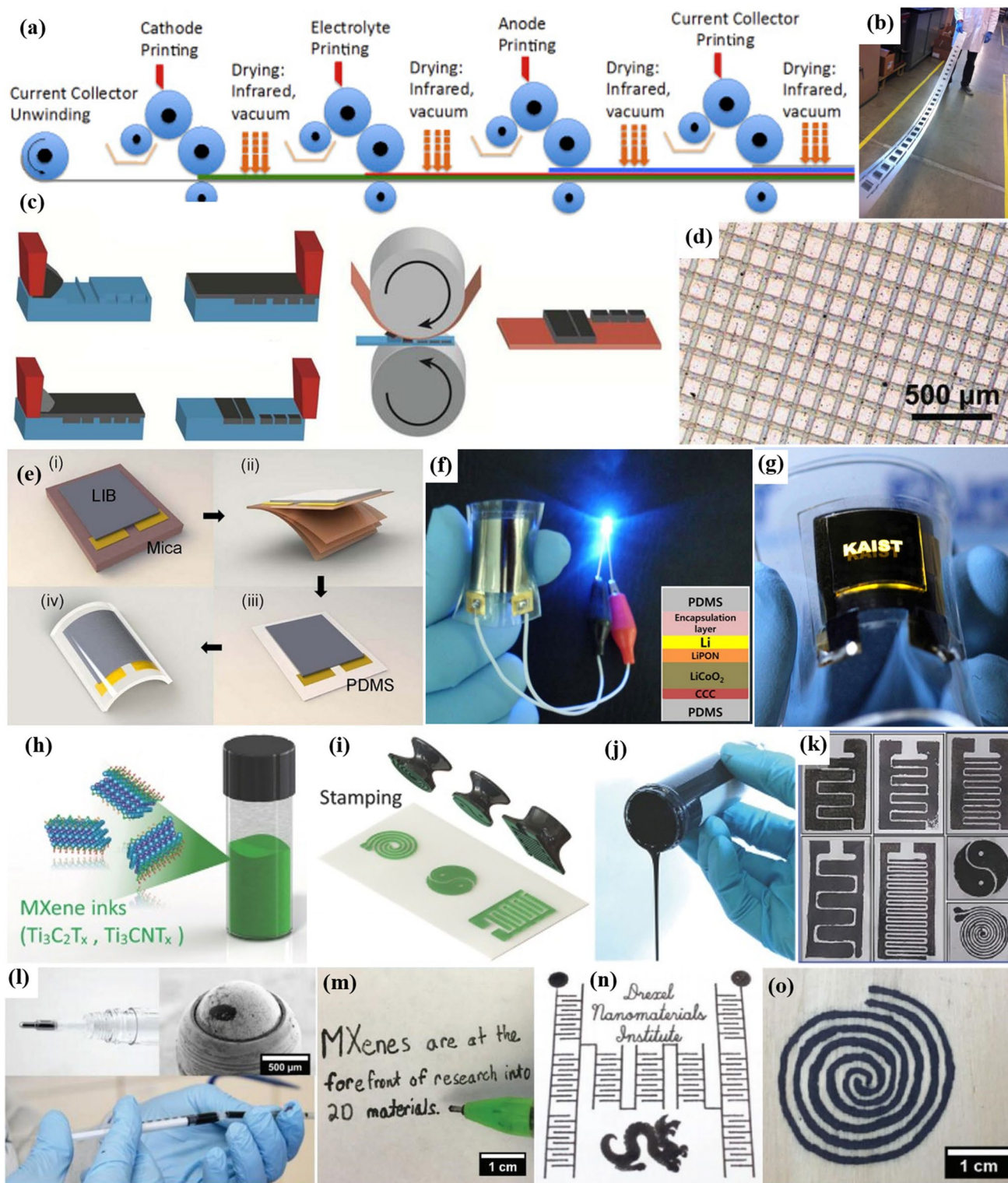
EESDs ($\sim 10^1 \mu\text{m}$) [54]. And although films produced from this printing method are not particularly suitable for the engineering of conventional EESDs because of the enormous time costs from the multiple repeated printing steps, flexographic printing is still regarded as a promising technique to prepare flexible EESDs for wearable electronics and smart packaging in the application of “Internet of things (IOT)” that requires low energy consumption because it is highly compatible with various substrates such as paper, plastic and textile [54]. Recently, in order to optimize the rheology, wettability and dispersal quality of flexographic-printed inks, Wang et al. [81] prepared a series of aqueous and organic MnO_2 cathode inks based on single modified styrene-butadiene rubber (PSBR) to obtain appropriate rheology and enabled the continuous flexographic printing of high-quality patterns (Fig. 10a, b). Further, an electrode film with an average thickness of $28 \mu\text{m}$ was obtained through multi-step repeated printing and the as-assembled cells using this MnO_2 film cathode and a Zn foil anode exhibited a capacity of 0.16 mAh cm^{-2} at a current density of 0.05 mA cm^{-2} .

Similarly, gravure printing is also a type of roll-to-roll printing technique in which a blade coating step is used to fill a pattern carrier with component ink (Fig. 10c). Here, the ink pattern is sequentially transferred to the target substrate through a normal roll-to-roll process in which the thickness of the gravure-printed films depends on the depth of the grooves, thereby providing opportunities for the one-step fabrication of printed films with thickness gradients in different sections, which is beneficial for the integration of multiple electronics on chips. For example, inspired by the ink preparation method for inkjet printing by Östling et al. [101], Secor et al. [82] developed stable, high-concentration and environmentally friendly graphene-based inks with tunable rheology and achieved uniform, large-areal gravure-printed graphene patterns on flexible substrates (Fig. 10d) in which by tailoring ink properties and printing conditions, high resolution of $\sim 30 \mu\text{m}$ and high electrical conductivity of $\sim 10000 \text{ S m}^{-1}$ were obtained in continuous graphene lines. Additionally, Xiao et al. [141] were also able to fabricate graphene-based interdigital MSCs using gravure printing, which provides numerous opportunities to integrate EESDs with power consumption devices such as sensors through a one-step printing technique.

Transfer printing is also a common on-contact printing technique that usually consists of several typical steps involving: (1) the preparation of designable patterns for functional materials on donor substrates and the adherence of a rate-sensitive elastomeric stamp on the substrate to cover these patterns; (2) the high-velocity peeling of the elastomeric stamp holding the objects to capitalize on the strong interaction between the objects and the stamp; (3) the contacting of the stamp and the receiving substrate; and (4)

the low velocity peeling of the elastomeric stamp to leave the objects on the receiving substrate [142]. Here, transfer printing can enable the large-area and high-resolution ($\sim 1 \mu\text{m}$) printing of various functional materials with a wide range of sizes and shapes on different substrates, especially patterned structures on donor substrates by means of other strategies including self-assembly, bottom-up growth, etching and sputtering. However, the complexity resulting from the multiple technologies increases costs and limits broad application. As an example, Koo et al. [143] used transfer printing to develop a bendable all-solid-state LIB (Fig. 10e–g) in which a sequent LBL deposition strategy based on sputtering and thermal annealing was used to prepare a Ni-alloy current collector, an LCO cathode, a lithium phosphorus oxynitride (LiPON) electrolyte, a Li metal anode and a protective encapsulation layer on a mica substrate. After that, the mica substrate was peeled off through physical delamination using sticky tape and transferred onto a flexible polydimethylsiloxane (PDMS) substrate and a flexible LIB was obtained after encapsulation with another layer of PDMS. And as a result, the LIB exhibited an energy density of 2.2 mWh cm^{-3} and favorable flexibility with only slight capacity loss under serious bending deformation. More importantly, an all-flexible device integrating the bendable LIB and a flexible LED was prepared and indicated the potential of the transfer printing technique in integrated systems. To further simplify the fabrication process, Zhang et al. [84] also developed a transfer printing strategy using patterned rigid stamps in which by combining 3D-printed patterned stamps with viscous aqueous MXene inks (Fig. 10h, i), planar MSCs with interdigital, spiral and “yinyang” geometry can be fabricated on different substrates (Fig. 10k). Benefiting from the intrinsic high capacitance and metallic conductivity of the MXene nanosheets, the as-prepared interdigital MSCs delivered an areal capacitance of 61 mF cm^{-2} at $25 \mu\text{A cm}^{-2}$, good rate capabilities with an areal capacitance of $\sim 50 \text{ mF cm}^{-2}$ while current density increased by 32 folds. Furthermore, a new printing strategy based on cylindrical stamps has been developed to rapidly fabricate MSCs, thus offering opportunities for the scalable fabrication of EESDs through transfer printing.

Pen writing, inspired by daily hand writing, is another class of simple and low-cost printing techniques to directly write functional material patterns onto target substrates using various pens including fountain pens, brush pens, rollerball pens and pencils [144] and has already been used in the fabrication of electrochemical sensors, transistors and EESDs [145–147]. In addition, pen writing is extremely suitable in the design and fabrication of “Do-it-Yourself” electronics because of ubiquitously available pens and simple processes. As a typical example, Quain et al. [148] developed high-concentration aqueous MXene inks (30 mg mL^{-1}) for commercially available pens to enable the direct writing



of conductive patterns on various substrates, including papers, plastic, clothes, woods and even fruits (Fig. 10l–o) in which the pen-written MSCs delivered an areal capacitance of 5 mF cm^{-2} without the need for any metal current collectors. Moreover, a modular device consisting of four

serially connected cells achieved a voltage of 2.4 V, thus demonstrating the remarkable performance customization of pen writing. Aside from the direct construction of micro-electrodes, pen writing can also be combined with metal coatings to achieve pen lithography [83, 149]. For example,

Fig. 10 Fabrication of batteries and SCs through flexographic printing, gravure printing, transfer printing and pen writing. **a** Schematic of the multi-step flexographic printing process for battery production. **b** Continuously printed cathode films on a piece of stainless steel foil. Reprinted with permission from Ref. [81]. Copyright 2014 Elsevier. **c** Schematic of the gravure printing process. **d** Gravure-printed graphene-based crossbar arrays. Reprinted with permission from Ref. [82]. Copyright 2014 John Wiley and Sons, Inc. **e** Fabrication process of bendable LIBs through transfer printing. **f** Photograph of a transfer-printed LIB in a bent state powering an LED. **g** Photograph of an all-in-one LED system with a bendable LIB. Reprinted with permission from Ref. [143]. Copyright 2012 American Chemical Society. **h** Schematic of MXene-based inks and **i** the printing process using stamps. Photographs of **j** MXene-based inks and **k** planar MSCs fabricated with 3D-printed patterned stamps. Reprinted with permission from Ref. [84]. Copyright 2018 John Wiley and Sons, Inc. **l** Images of a rollerball pen used for the direct writing of MXene ink. **m** Pen writing of MXene ink on paper. **n** Arrays of MXene-based MSCs written on paper. **o** A spiral MXene circuit pattern written on wood. Reprinted with permission from Ref. [148]. Copyright 2019 John Wiley and Sons, Inc.

Jiang et al. [83] used pen-writing structures as sacrificial patterns to electrodeposit PANI and MnO_2 as electrode materials in aqueous solution and etched the patterns in acetone or alcohol to take advantage of the solubility difference of commercially available pen inks to fabricate patterned MSCs, which was successfully demonstrated on rigid, flexible and even curved substrates, indicating great applicability. Pen writing can also be applied in the fabrication of conductive connects for integrated power sources. For example, Zhi et al. [150] obtained integrated ppy-based MSCs by simply drawing conductive connecting wires between MSCs, thus largely reducing process complexity and improving feasibility on various substrates. Despite these promising finding however, great barriers exist for pen writing towards industrial application due to limited resolution and uniformity.

3 Form Factors and Functionalities of Printed EESDs

Due to abundant advantages including low-cost instruments, simple operation processes and loose working condition requirements, printing technologies have been widely researched to bridge achievements in laboratories to industrial settings and possess great potential in the scalable fabrication of high-performance EESDs. Here, aside from the need for electrochemical performance improvements, future EESDs are highly required to possess various form factors and functionalities, including designable and customized shapes, mechanical flexibility, stretchability and robustness as well as enhanced safety and optimal integration levels to match the properties of future energy consumption devices. In this respect, printing techniques also show great potential due to superior process flexibility, and in this section, the

form factors and functionalities of printed EESDs will be discussed.

3.1 Mechanical Flexibility, Stretchability and Robustness

The rapid development of electronic products such as phones, computers and cameras has significantly altered everyday lifestyle in past several decades, and in next decade, it is predicted that flexible and wearable electronics such as flexible phones, wearable interactive glasses and patchable health sensors will become increasingly main stream and place severe demands on EESDs to possess not only higher energy densities but also more compatible mechanical properties to maintain stable performances in complex deformation states of bending, twisting and stretching.

Here, the outstanding compatibility of printing techniques with various substrates can allow printed EESDs to directly inherit the mechanical characteristics of target substrates and can provide great conveniences in the construction of flexible, stretchable and robust EESDs. For example, spray-coated MSCs based on hybrid inks of EG and PH1000 on an ultrathin PET substrate fabricated by Liu et al. [90] can be attached to fingers or other body parts and exhibit excellent compatibility with finger movements and favorable mechanical flexibility with negligible capacitance degeneration after 1000 bending cycles (Fig. 11a–c) due to the intrinsic flexibility of the PET and the 2D graphene nanosheets along with the in-plane separator-free interdigital geometry. Aside from bending, stretching is another typical mechanical deformation occurring on human skin. Based on this, Kumar et al. [78] developed stretchable $\text{Zn-Ag}_2\text{O}$ batteries on a highly stretchable thermoplastic polyurethane substrate using a multi-step screen printing process (Fig. 11d) in which the as-fabricated $\text{Zn-Ag}_2\text{O}$ batteries achieved a stable reversible capacity of 2.5 mAh cm^{-2} even after multiple 100% stretching processes because of the use of a hyper-elastic polystyrene-block-polyisoprene-block-polystyrene (SIS, ~1300% elongation) material as a binder in the preparation of the printed ink, thus demonstrating the tremendous potential of screen printing in the fabrication of wearable power sources (Fig. 11e, f). In another example, Lee et al. [151] prepared an electronic garment with a bulb-shaped SC through the UV-assisted multiple screen printing of AC-CNTs electrodes and an ionic liquid electrolyte followed by encapsulation with a water-proof packaging film and further connection with an LED. The resulting screen-printed electronic garment was able to effectively maintain the normal operation of the LED in various mechanical and thermal stress situations including wringing, folding, ironing (~140 °C) and laundering (Fig. 11g-i), thus exhibiting the great applicability of printing methods towards various daily activities. Furthermore, Shi et al. [152] fabricated self-healable

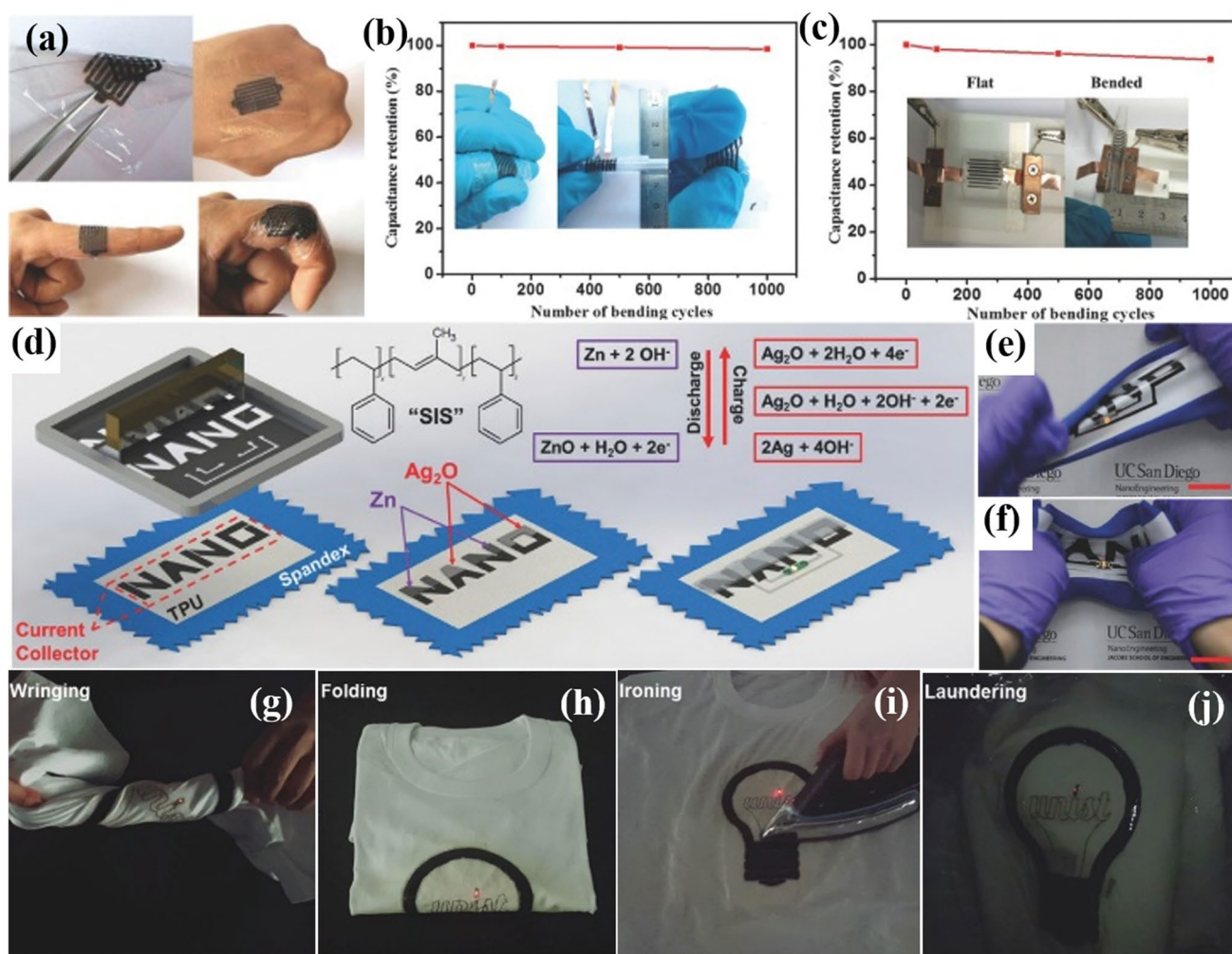


Fig. 11 Flexibility, stretchability and robustness of printed batteries and SCs through the directly inherited mechanical properties of substrates. **a** Photographs of spray-coated MSCs on ultrathin PET attached to a finger. Capacitance retention of MSCs after 1000 times of bending using **b** ultrathin and **c** regular PETs. Reprinted with permission from Ref. [90]. Copyright 2016 John Wiley and Sons, Inc. **d** Schematic of the screen printing of a Zn-Ag₂O battery on a stretch-

able textile. Photographs of a sealed battery in **e** twisted and **f** strained states. Reprinted with permission from Ref. [78]. Copyright 2017 John Wiley and Sons, Inc. **g–j** Photographs of a T-shirt with a printed SC upon exposure to various stress modes (wringing, folding, ironing and laundering) encountered in daily use. Reprinted with permission from Ref. [151]. Copyright 2018 John Wiley and Sons, Inc.

MSCs through directly printing CNT electrodes onto ionogel electrolyte films with a dual-dynamic network composed of Li⁺-poly(ethylene oxide) (PEO) and hydrogen bonding. Attributed to superior high tensile fracture strength and the stretchable and self-healable properties of the electrolyte film, the capacitance retention of the resulting MSCs reached 98% after 5 repeated cutting cycles to demonstrate outstanding reliability and robustness.

Aside from inheriting substrate properties, printing technologies can also construct flexible and stretchable EESDs through structural design. For example, Kim et al. [153] developed integrated array MSCs with an island-bridge structure utilizing long and narrow serpentine metallic wires as interconnections and spray-coated CNTs as electrodes on

PDMS substrates (Fig. 12a) and reported that the delicate structural design enabled decoupled energy storage and mechanical properties in an integrated EESD, thus leading to stable performances in different deformation states of bending and stretching (Fig. 12b, c) and exhibiting the great potential of the construction of flexible and wearable EESDs through geometric design with printing techniques. More interestingly, the combination of rational design and printing techniques can also endow inorganic ceramic electrolytes with favorable flexibility. For example, Xie et al. [154] recently developed a flexible Li_{6.75}La₃Zr_{1.75}Ta_{0.25}O₁₂ (LLZO) garnet electrolyte membrane with a novel tile-and-grout structure using 3D printing (Fig. 12d, e) in which a parametric finite element analysis was first conducted to

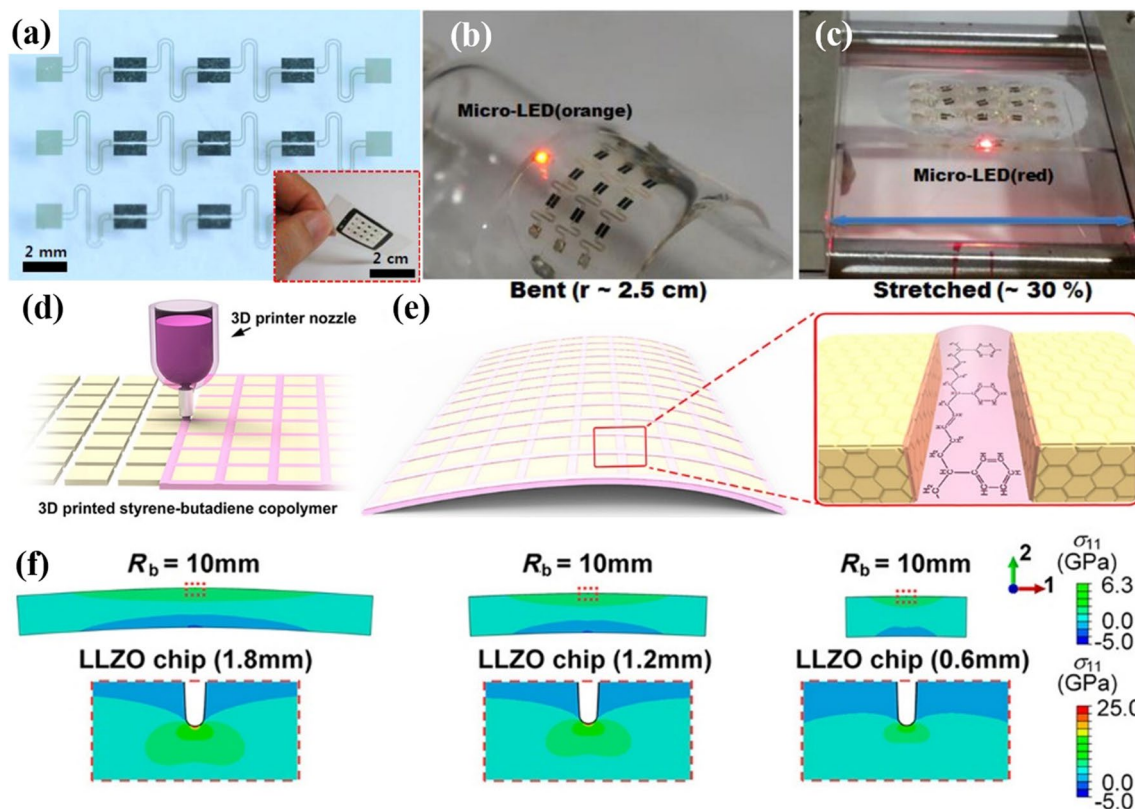


Fig. 12 Flexible printed batteries and SCs through structural design. **a** Photographs of integrated MSC arrays with an island-bridge structure on a stretchable PDMS substrate. **b, c** Photographs of the array MSCs lighting an LED in bending and stretching states. Reprinted with permission from Ref. [153]. Copyright 2013 American Chemical Society. **d** 3D-printed SBC ink used to firmly bind neighboring

LLZO chips together. **e** Resulting flexible LLZO electrolyte with a tile-and-grout design. **f** Stress analysis of 200 μm thick LLZO chips with different side lengths under the same bending radius (10 mm). Reprinted with permission from Ref. [154]. Copyright 2017 American Chemical Society

investigate the crack formation process based on the fracture mechanics and mechanical properties of LLZO. Here, by comparing the deformation strain energy and the surface energy (serving as driving force of crack growth and resistance to fracture progression, respectively) of the LLZO chip with different size lengths in various bending states in their analysis model (Fig. 12f), the critical value of the LLZO chip size in every bending state was obtained. And to further verify the calculation results, they conducted experiments employing round LLZO pellets in different states and found that the resultant average values of the size distribution were clearly lower than the calculated critical value, demonstrating the favorable consistency between theoretical prediction and experimental results. And based on these theoretical and experimental optimization results, these researchers fabricated an LLZO membrane with a tile-and-grout structure through the 3D printing of a styrene-butadiene copolymer (SBC) ink as a binder to glue LLZO chip arrays together. As a result, the as-prepared LLZO membrane showed better flexibility than common polyethylene oxide-based polymer electrolyte membranes and enhanced cycling capability in

symmetric Li/Li cells, demonstrating the viability of printing techniques in the fabrication of flexible EESDs through structural design.

3.2 Shape Diversity and Customization

To satisfy the demand for aesthetic diversity and shape customization in emerging consumer electronics, future EESDs need to be conformable and seamlessly integrated within these electronics. Here, printing techniques that can produce high-resolution texts and patterns on various substrates are naturally expected to fabricate EESDs with excellent shape diversity and customization.

As a typical example, Zheng et al. [74] prepared arbitrarily shaped (e.g., the junction wire, the hollow square, the letter “A”, numbers “1” and “2”) planar stacked MSCs through the consecutive spray coating of EG and nanosized GO dispersions as electrodes and ultrathin separators, respectively (Fig. 13a–c) based on conformable shadow masks for electrodes and the separator and found that the resulting MSCs with various shapes all produced ideal electrical

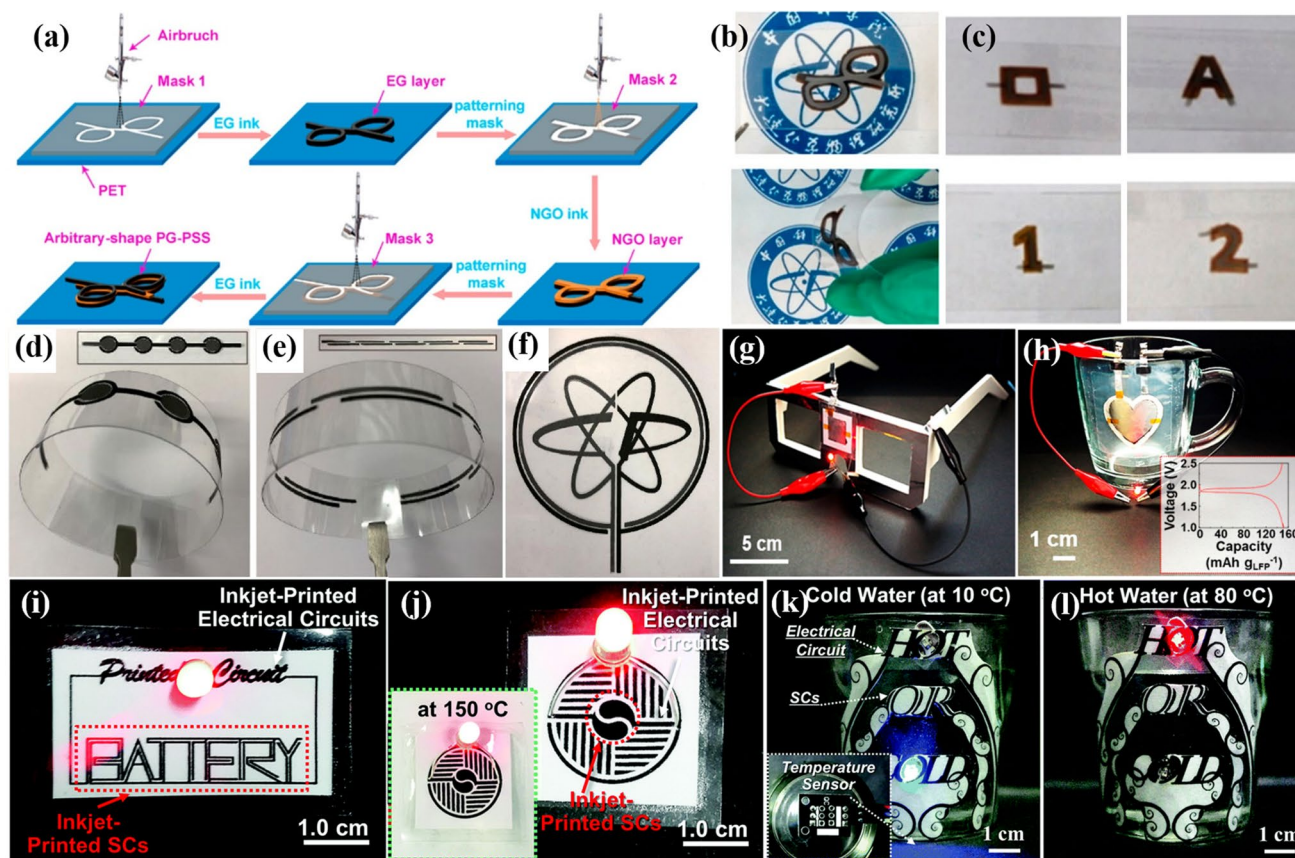


Fig. 13 Customization, conformability and aesthetics of printed batteries and SCs. **a** Fabrication schematic of arbitrarily shaped planar stacked MSCs made up of an EG/GO/EG layer-structure film on a PET substrate through spray coating. **b** Photographs of a junction-wire-shaped MSC in flat and bending states. **c** Photographs of MSCs with various geometry of hollow square, “A”, “1” and “2” shapes. Reprinted with permission from Ref. [74]. Copyright 2017 American Chemical Society. **d–f** Photographs of screen-printed **d** concentric-circle-shaped, **e** linear-shaped and **f** “DICP” logo Zn/MnO₂ batteries. Reprinted with permission from Ref. [155]. Copyright 2019 Oxford University Press. **g** Photograph showing a screen-printed LIB on paper-made eyeglasses powering an LED. **h** Photograph showing a

screen-printed heart-shaped LIB on a curvilinear glass surface powering an LED. Reprinted with permission from Ref. [112]. Copyright 2017 American Chemical Society. **i** Photograph of an inkjet-printed letter-shaped SC seamlessly connected with inkjet-printed electrical circuits and an LED. **j** Photograph of an inkjet-printed symbol-shaped SC seamlessly connected with inkjet-printed electrical circuits and an LED. **k, l** Photographs depicting the operation of a smart system composed of a tandem inkjet-printed letter-shaped “OR” MSC, electrical circuits and a temperature sensor for **k** cold water (~10 °C) and **l** hot water (~80 °C). Reprinted with permission from Ref. [75]. Copyright 2016 The Royal Society of Chemistry

double-layer capacitive behaviors, thus demonstrating the superior shape applicability of spray-coated MSCs. Furthermore, Wang et al. [155] successfully prepared more diversified and aesthetically varied patterned microscale aqueous Zn–MnO₂ batteries (e.g., linear, concentric circle and the logo of “Dalian Institute of Chemical Physics” geometry) through the screen printing of graphene-based current collector inks, Zn-based anode inks and MnO₂-based cathode inks (Fig. 13d–f). In particular, the successful demonstration of the logo-shaped microbatteries demonstrated the excellent opportunity of the production of trademark-conformable EESDs on clothing, which possesses outstanding commercial prospects. Despite the results in these two studies however, the conformable deposition of electrolytes was not achieved in either. In this respect, Kim et al. [112]

incorporated UV-sensitive monomers into electrolyte and electrode slurries to prepare printable inks and constructed quasi-solid-state LIBs based on LFP cathodes and LTO anodes through UV-assisted LBL screen printing. Here, as a demonstration of outstanding shape customization, a printed conformal LIB was directly fabricated on model eyeglasses (Fig. 13g) and a heart-shaped LIB was successfully fabricated on a curvilinear transparent glass surface to deliver a stable voltage platform and a high capacity of ~150 mAh g⁻¹ (Fig. 13h), thus demonstrating the excellent shape diversity and process superiority of screen printed EESDs. More succinctly, Choi et al. [75] were able to fabricate mask-free all-inkjet-printed solid-state MSCs with superior shape diversity and customization on PET and paper substrates and reported that not only limited to letter-shaped MSCs,

artistically integrated circuits can also be simultaneously inkjet printed on papers and seamlessly connected with inkjet-printed MSCs to power LEDs (Fig. 13i, j). Moreover, combining the advantages of the high thermal stability of the CNTs/AC electrodes and the ionic liquid electrolyte, the inkjet-printed MSCs can exhibit stable performances at a high temperature of 150 °C (Fig. 13j). More significantly, the all-inkjet-printed MSCs can be used as power sources to construct smart glass cups by incorporating temperature sensors into the integrated circuit to intelligently display information concerning hot or cold water, disclosing superior potential as aesthetic EESDs for future IOT.

Despite these advancements in shape-customized printable EESDs, discussions into the effects of electrode structure on electrochemical performance in planar EESDs remain lacking [79, 156]. And although the electrochemical performance of planar EESDs can generally be enhanced by narrowing the microelectrode width and interspacing between adjacent electrodes based on research on interdigital MSCs [41, 85], to accurately illustrate the relationship of structure and performance, *in situ* characterization techniques and quantized models are highly still required for the fundamental understanding of ion transport dynamics in various electrode geometry to guide device design.

3.3 Integration

Because the output voltage and current of single EESDs are limited, the development of integrated EESDs with tailored voltages and currents is necessary to meet the strict demands of different electronics in various applications [79, 157, 158]. However, the traditional integration strategy of connecting multiple cells in series and/or in parallel using metal wires is unsuitable for microscale EESDs, especially flexible and wearable EESDs, due to heavy weights, large volumes, complex connection steps and incompatible mechanical properties at the interfaces of electrodes and metal wires [90, 159]. Therefore, it is necessary to develop all-in-one integrated EESDs for application in future electronics [160, 161]. Printing technologies, with great advantages in LBL deposition, pattern construction and process flexibility, are considered as a kind of competitive strategies to fabricate integrated EESDs. In addition to self-integration, the integration of energy harvesting devices (e.g., solar cells, nanogenerators) and energy consumption devices (e.g., environment sensors, health monitors) with EESDs to construct self-powered, maintain-free and standalone energy systems [162–165] is another increasingly important developmental direction that can simultaneously overcome the discontinuity and instability of energy harvesting devices and provide energy for EESDs [24]. Here, printing technologies have also exhibited tremendous prospects due to their powerful ability to construct highly conductive circuit platforms for

different modules in integrated systems and possibility used to realize seamless integration between printable EESDs and printable electronics through similar preparation processes.

Recently through the elaborated design of device geometry, Shi et al. [85] developed linear tandem planar MSCs using highly conductive EG/PH1000 hybrid ink as current collectors, microelectrodes and interconnects through a one-step spray coating process with the assistance of shadow masks and reported that the resulting modular energy storage pack consisting of 10 serially connected MSCs operated stably at a high voltage of 8 V, showing great potential as microscale power sources in high-voltage electronics. In this study, high-capacitance and high-energy MSCs were also fabricated by incorporating pseudocapacitive PANI-graphene electrode materials and constructing asymmetric MSCs based on EG and MnO₂/PH1000 as negative and positive electrodes, respectively, again demonstrating the outstanding universality and flexibility of the spray coating technique. In another example, Li et al. [111] further improved integration by developing an EG ink with ethyl cellulose as a stabilizer through a solvent exchange process for inkjet printing (Fig. 14a). Due to the high electrical conductivity and intrinsic capacitance of the ink, the resulting EG films can simultaneously serve as current collectors and microelectrodes after the removal of ethyl cellulose through annealing in air. Then, a polyelectrolyte ink based on poly(4-styrenesulfonic acid) (PSSH) was also prepared to realize full inkjet-printed MSCs (Fig. 14a). Because of the high quality of inks and scalability of inkjet printing, modular MSCs consisting of hundreds of individual cells with arbitrary serial/parallel connections can be successfully obtained (Fig. 14b) to achieve controllable voltage and current output. Here, the resulting integrated MSCs [12S × 12P, 12S and 12P represent the number of cells connected in series (S) and in parallel (P)] operated stably at a high voltage of 12 V (Fig. 14c, d), indicating great potential as integrated power sources. Despite these advancements however, the simple and rapid fabrication of highly integrated EESDs has yet to be fully achieved. To address this, Shi et al. [79] developed a simple, cost-effective and scalable screen printing technique for the rapid fabrication of highly integrated MSCs based on highly conductive graphene-based inks and reported that the construction of integrated MSCs composed of hundreds of single cells can be achieved within a few seconds without the need for any post-treatment steps, greatly reducing fabrication times and enhancing fabrication efficiency for highly integrated EESDs. In addition, as-obtained integrated MSCs (10S × 1P) in this study exhibited a nearly rectangular CV curve and symmetric triangular GCD results at a high voltage of 8 V and MSCs (10S × 2P, 10S × 5P) displayed nearly proportionally increased capacitance and decreased equivalent series resistance (Fig. 14e–h), demonstrating ideal serial and parallel capacitive behaviors. Furthermore, a

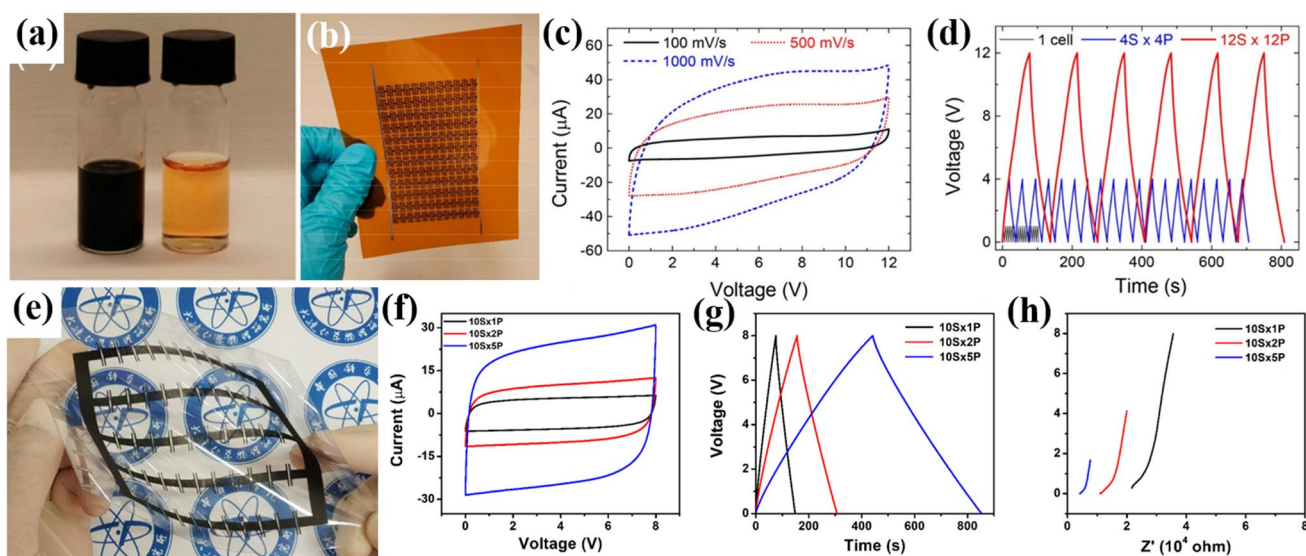


Fig. 14 Self-integrated printed EESDs. **a** Photograph of EG ink (left) and PSSH ink (right) used to inkjet-print electrodes and electrolytes. **b** Photograph of inkjet-printed integrated MSCs (12S×12P). **c** CV curves of the inkjet-printed MSCs (12S×12P) tested at different scan rates. **d** GCD curves of inkjet-printed MSCs (12S×12P, 4S×4P and 1S×1P) tested at a current of 10 μA . Reprinted with permis-

sion from Ref. [111]. Copyright 2017 American Chemical Society. **e** Photograph of screen-printed MSCs (10S×5P) in the bending state. **f** CV curves obtained at 200 mV s^{-1} , **g** GCD profiles tested at 3 μA and **h** the complex plane plot of the screen-printed MSCs (10S×1P, 10S×2P and 10S×5P). Reprinted with permission from Ref. [79]. Copyright 2019 The Royal Society of Chemistry

highly integrated MSC pack consisting of 130 in-series cells in this study operated stably at an ultrahigh voltage of more than 100 V, which is the highest value reported for printable SCs, again indicating the superior integrity and performance uniformity of screen-printed MSCs.

Aside from inner modularization, integration between printed EESDs and energy consumption or energy harvesting modules has also been intensively investigated. For example, Xu et al. [166] fabricated asymmetric SCs using $\text{Ti}_3\text{C}_2\text{T}_x$ MXene and Co-Al layered double hydroxide as the negative and positive electrodes, respectively, through a two-step screen printing process with sputtered interdigital Au current collectors and reported that the resulting SC exhibited a wider voltage window of 1.45 V as compared with MXene-based symmetric SCs (~ 0.6 V) and a high energy density of $8.84 \mu\text{Wh cm}^{-2}$. These researchers also used the screen-printed asymmetric SCs to power a force sensor to build a portable integrated system on one chip and reported similar response signals as compared to that powered by an external bias in different applied pressures, implying the reliability of printed SCs as power sources for other electronics. Printable EESDs can also readily be integrated with energy harvesting devices, which is considered to be the ultimate energy sources for EESDs, especially for maintain-free application. For example, Um et al. [167] developed a prototype self-powered integrated system through the LBL screen printing of quasi-solid-state LIBs onto the Al electrodes of silicon-based photovoltaic cells (Si-PV) based on

a UV curing process to simultaneously achieve the electrical-architectural integration of the two different energy systems. Moreover, the working voltage of LIBs can easily be adjusted through the design of the interior serial structure by sharing a thin Al foil as the current collectors for two adjacent single cells (Fig. 15a), which can tailor performance, enhance the integrity of the self-powered system and match the open-circuit voltage of the Si-PVs based on target applications. The resultant system was able to deliver high photoelectrical conversion/storage efficiency of 7.61% and sustain its capacity even after 100 photo-charge/discharge cycles and continuous discharge capacity at a high rate of 28 C under sunlight illumination (Fig. 15c–e). Moreover, this integrated system (~ 0.13 cm) was able to be embedded into a smartcard without altering the shape and dimension of the card due to its ultrathin thickness (Fig. 15b), indicative of its great potential as maintain-free power sources for IOT. In another example, Fan et al. [165] proposed a hybrid system with a higher degree of integration composed of energy harvesting, energy storage and energy consumption devices (solar cells, MSCs and gas sensors) in which an Ag-based integrated circuit, MnO_2 -rGO-PH1000-based MSCs and SnO_2 -based sensors were inkjet-printed on a PET substrate in sequence utilizing respective inks with an amorphous silicon solar cell being embedded into the integrated circuit (Fig. 15f). The harvested solar energy can be used to directly power the SnO_2 sensors or be stored in the inkjet-printed MSCs and then released as needed, enabling

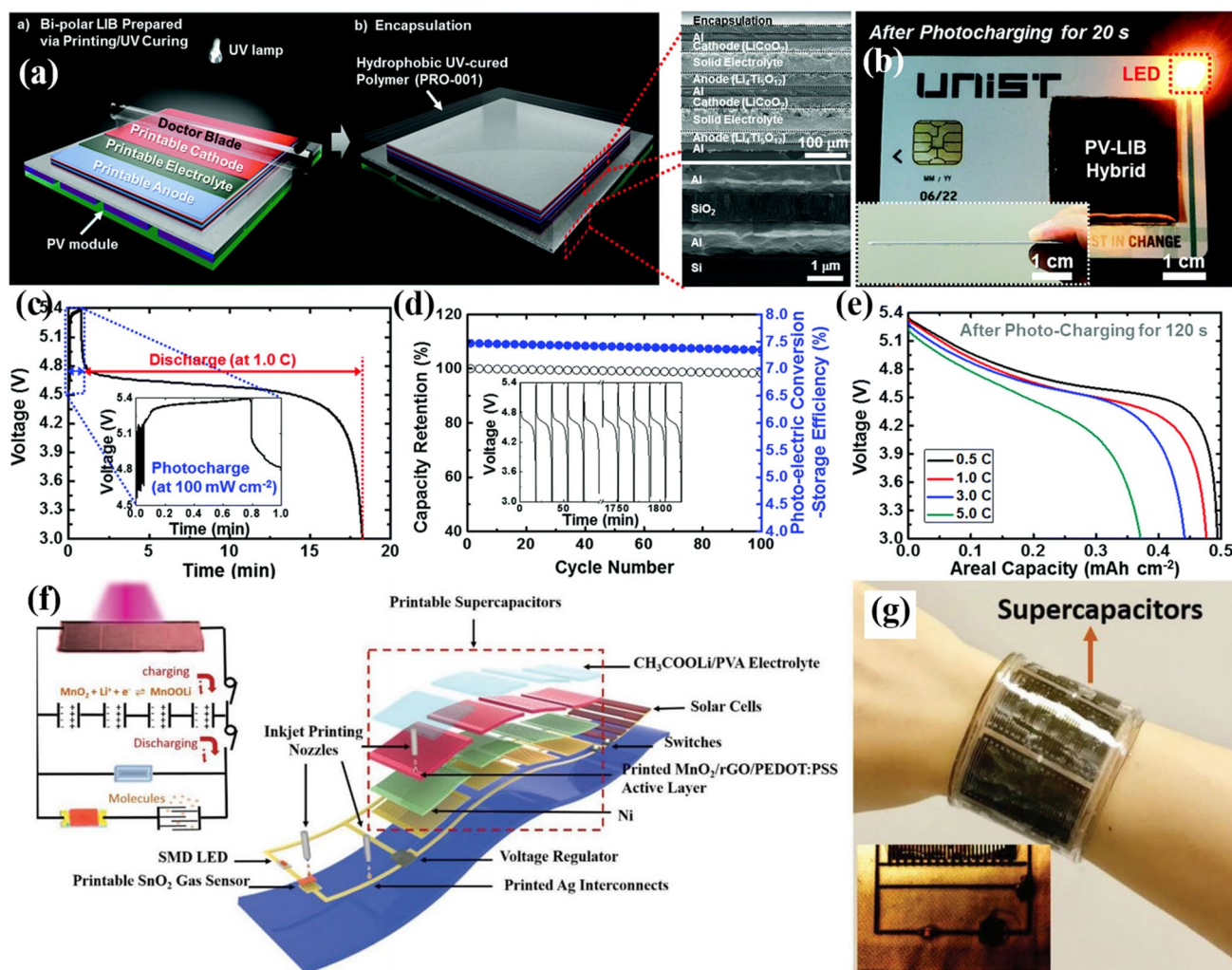


Fig. 15 Self-powered integrated systems composed of printed EESDs, energy harvesters and energy consumption devices. **a** Schematic of the screen printing-based stepwise fabrication of an LIB cell on a SiPV module (left) and cross-section SEM images of a 2-stack LIB cell and the seamlessly unitized interface between the LIB and the SiPV module (right). **b** Photograph showing the operation of an integrated SiPV-LIB-embedded smartcard. Inset shows the thickness of the smartcard. **c** Photo-charge curve under a light intensity of 100 mW cm⁻² and the galvanostatic discharge profile at 1.0 C of the SiPV-LIB device. **d** Photo-charge/galvanostatic discharge cycling performance and photoelectric conversion/storage efficiency of the

SiPV-LIB device. **e** Galvanostatic discharge rate capability of the SiPV-LIB device at different discharge current densities from 0.5 to 5.0 C. Reprinted with permission from Ref. [167]. Copyright 2017 The Royal Society of Chemistry. **f** Schematics of the inkjet printable fabrication procedure and the operational mechanism (inset) for a flexible monolithically integrated self-powered smart sensor system on a plastic substrate. **g** Photograph of a printed monolithically wristband-shaped integrated self-powered sensor system. Inset: LED as an indicator for gas detection. Reprinted with permission from Ref. [165]. Copyright 2019 John Wiley and Sons, Inc.

the facile construction of a fully integrated, self-powered and maintain-free wearable wristband-shaped gas sensor system (Fig. 15g). While exposed to high-concentration ethanol or acetone, the SnO₂ sensors would exhibit obvious resistance drops and enable an LED indicator to light up and send warning signals. Despite these results, the performance of printed MSCs and the sensitivity of printed sensors are expected to further improve toward actual application in the future. In addition, the integration of EESDs in electronic systems to simultaneously act as power sources and other

functional elements is a delicate strategy to improve both energy density and integrity in devices [168].

4 Challenges and Prospective

Although great advancements have been achieved for printed power sources including batteries and SCs in terms of continuously enhanced performances (e.g., energy density, power density and cycle stability) and various form factors

(e.g., designable sizes and shapes, aesthetic properties, miniaturization, flexibility, stretchability and integration) (as briefly summarized in Table 2), the development of printable EESDs is still in initial stages. Because of this, systematic optimizations and overall improvements are needed for components (e.g., electrodes, electrolytes, current collectors, separators, package and interconnects), device configurations, component ink rheological properties and encapsulation techniques to achieve actual application.

Before printable EESDs can achieve commercialization, several challenges must be addressed. First, the electrochemical performance of printable EESDs requires further improvement to satisfy severe application demands. With regard to this, several promising strategies exist: (1) the latest advancements in conventional battery and SC systems should be introduced to printable EESDs for performance enhancement such as high-capacity electrode materials (e.g., Si anodes, MXene) [169], high energy density battery and SC systems (e.g., Li metal batteries, Li–S/air batteries, pseudocapacitors and hybrid capacitors including lithium ion capacitors and potassium ion capacitors) [29, 170–174] and high-voltage electrolytes (e.g., water-in-salt and solvent-in-salt electrolytes, ionic liquids) [18, 50]; (2) because high-content inactive and nonconductive rheological additives can reduce the electrochemical performance of printed EESDs [79], the development of rheological agents with significant effects through trace-amount additions or high electrical conductivity is needed to maximize active material ratios and increase rate performances in case of smooth printing processes; (3) high-resolution printing techniques need to be developed to reduce the thickness of separators in stacked EESDs, narrow the interspacing between the cathode and anode of planar EESDs and lighten and thin encapsulation materials to maximize the active material ratios and increase the gravimetric and volumetric energy densities of printable EESDs at the device level [2, 120]; (4) the outstanding patterning ability of printing techniques needs to be fully utilized to construct advanced electrode configurations such as 3D array microelectrodes to increase aspect ratios and further improve energy and power densities.

As another challenge, most studies on printable EESDs have neglected the aspect of form factors including customized sizes and shapes, aesthetic properties, miniaturizations and flexibility, thus resulting in limited configuration diversity and functionality [175, 176]. To overcome this, high-resolution and mask-free digital printing techniques need to be developed for the scalable fabrication of designable patterned electrodes to endow EESDs with aesthetically appealing and high-performance properties. In terms of smoother printing processes, polymer-based electrolytes that possess high ionic conductivity, flexibility, stretchability or self-healing properties as well as tailored rheology are crucial in the preparation of portable and wearable EESDs

[177]. In addition, the fabrication of flexible printed EESDs through rational structural design remains underdeveloped, indicating there existed great unexplored space in fabrication of flexible EESDs through the combination of advanced geometry designs and printing technologies. Furthermore, research concerning printable current collectors has lagged behind in comparison with electrodes, electrolytes and separators, which has gradually become the bottleneck in the parallel development of all-printable EESDs. Therefore, more efforts need to be devoted to the development of carbon or metal powder-based inks with tunable viscosity and rheology in the fabrication of printable current collectors. Here, researchers have reported that high-performance and electrically conducting materials (e.g., graphene, CNTs and MXene inks in SCs and Zn inks in Zn ion batteries) can be used as current collectors and electrodes simultaneously [178], which can greatly simplify the printing process and improve the form factors of printed EESDs.

In addition, although self-integrated printed EESDs and integrated electronic devices powered by printed EESDs are important devices, they remain underdeveloped. Here, planar EESDs have shown great advantages in terms of both self-integration and external integration due to their advanced device structure involving positive and negative electrodes on one substrate. Based on this, the combination of highly conductive inks and high-resolution printing techniques to prepare patterned films, simultaneously acting as current collectors and interconnects in self-integrated planar EESDs is a promising and reliable strategy [159]. Furthermore, the development of rapid and scalable printing strategies to fabricate modular energy packs, especially within limited volume or area, consisting of several to hundreds of single cells connected in well-designed serial and parallel arrangements is key for the tailoring of voltage and current output to meet actual application requirements [74, 79]. Moreover, highly conductive printed patterned films can also act as platforms for EESDs, energy consumption devices and even signal transmission modules in integrated circuits and are not limited to the self-integration of EESDs. The sharing of substrates, current collectors and encapsulation materials in printable EESDs with flexible electronics is also an extremely attractive strategy because it can effectively accelerate the perfect integration of flexible systems, enhance the energy density and eventually contribute to the diverse form factors of printable EESD at the device level [36], in which the prerequisite is that their fabrication processes are compatible with each other. Alternatively, self-powered and maintenance-free electronics are necessary in a variety of applications (e.g., environmental sensors, IOT and implantable medical devices) [179] and the integration of energy harvesters (e.g., solar cells, nanogenerators) with printable EESDs to construct dual power sources that can allow for the conversion of solar energy or mechanical

Table 2 Recent advancements of printable EESDs in terms of performance and form factors

Printing technique	EESD systems/ electrodes	Rheological additive	Electrolyte/ separator	Voltage (V)	Thickness (μm)/ anode–cathode	Capacity/capacitance	Energy density	Features	Ref.
Spray coating	LIBs/LTO-LCO	PVDF	Kynarflex-PVDF-SiO ₂	1.5–2.7	109–143	120 mAh g ⁻¹	–	Curved surface	[64]
	SCs/EG	–	Nanosized GO	0–0.8	0.7	10.6 F cm ⁻³	0.98 mWh cm ⁻³	Arbitrary shapes	[74]
	SCs/EG-PH1000	–	PVA/H ₂ SO ₄	0–1	0.025	155 F cm ⁻³	12 mWh cm ⁻³	AC-line filtering	[89]
	SCs/EG-PH1000	–	PVA/H ₂ SO ₄	0–0.8	3.16	15.5 F cm ⁻³	1.38 mWh cm ⁻³	Self-integration	[85]
Inkjet printing	LIBs half-cell/ Si	PEDOT:PSS	LiPF ₆ in FEC:DMC	0–1	1	2500 mAh g ⁻¹	–	–	[95]
	SCs/ PEDOT:PSS	Triton-X 100	PVA/H ₃ PO ₄	0–0.8	–	1.13 mF cm ⁻²	–	Transparent	[97]
	SCs/AC-CNTs	SDBS, ETPTA	BMIMBF ₄	0–2	1.69	100 mF cm ⁻²	15 Wh kg ⁻¹	All-print, esthetics	[75]
	SCs/EG	Ethyl cellulose	PSSH	0–1	0.7	0.7 mF cm ⁻²	1 mWh cm ⁻³	Self-integration	[111]
	SCs/MnO ₂ , rGO	PEDOT:PSS	PVA/CH ₃ COOLi	0–0.8	2.5	12.9 mF cm ⁻²	–	Integration	[165]
Screen printing	LIBs/LTO-LCO	PVDF-HFP, ETPTA	LiBF ₄ in SBN, PVDF-HFP, ETPTA, Al ₂ O ₃	1.5–2.7	41.7–34.0	130 mAh g ⁻¹	–	Flexible, shape-variant, non-flammable	[77]
	Zn–Ag ₂ O batteries	Methylcellulose, PVA	KOH/PEO, acrylic acid	1–1.55	141–153	5.4 mAh cm ⁻²	–	–	[113]
	Zn–MnO ₂ batteries	Polyurethane resin	2 M ZnSO ₄ and 0.5 M MnSO ₄	0.9–1.8	6.4–9.8	19.3 mAh cm ⁻³	17.3 mWh cm ⁻³	Customized shapes	[155]
	SCs/graphene	P-VC/VAc	EMIMNTF2	0–0.8	5	0.89 mF cm ⁻²	1.81 mWh cm ⁻³	Self-integration	[79]
	SCs/activate carbon–Ag@ polypyrrole@MnO ₂	Waterborne resin	PVA/Na ₂ SO ₄	0–1.6	–	95.3 mF cm ⁻²	0.0337 mWh cm ⁻³	Stretchable	[109]
	SCs/ RuO ₂ ·xH ₂ O, rGO	GO	PVA/KOH	0–1	0.71	338 F cm ⁻³	18.8 mWh cm ⁻³	–	[110]
	Zn–Ag ₂ O	SIS	PAA/KOH, LiOH	0.8–2.3	–	2.5 mAh cm ⁻²	–	Stretchable	[78]
	SCs/AC, CNTs	TMPPT, TMPTA	LiTFSI in EMIMTFSI	0–1.5	–	74.2 mF cm ⁻²	–	Robust	[151]
3D printing	LIBs/LTO-LFP	GO	LiPF ₆ in EC/DEC, PVDF-HFP, Al ₂ O ₃	1–2.5	1060	100 mAh g ⁻¹	–	–	[118]
	LIBs/LTO-LFP	PVP	LiTFSI in PC, Al ₂ O ₃ , TX-100, ETPTA	1–2.5	1000	17.3 mAh cm ⁻³	20 mWh cm ⁻³	All-printed	[120]

Table 2 (continued)

Printing technique	EESD systems/ electrodes	Rheological additive	Electrolyte/ separator	Voltage (V)	Thickness (μm)/ anode–cathode	Capacity/capacitance	Energy density	Features	Ref.
	Li–O ₂ batteries/porous graphene cathode	–	LiTFSI in DMSO	Controlled discharge depth	–	–	–	–	[126]
	Zn–MnO ₂ batteries	PVDF–HFP	Zn ⁺ Tf [–] in BMIM ⁺ Tf [–]	1–2	total: 80–120	0.98 mAh cm ^{–2}	1.2 mWh cm ^{–3}	–	[122]
	SCs/graphene	CaCl ₂	1 M H ₂ SO ₄	0.8	300	213 F g ^{–1}	–	–	[133]
	SCs/MnO ₂ @graphene	Hydroxypropyl methylcellulose	3 M LiCl	0–0.8	4000	44.13 F cm ^{–2}	1.56 mWh cm ^{–3}	–	[80]
	SCs/rGO–GO/PANI	PEDOT:PSS	PVA/H ₃ PO ₄	0–1.2	80	19.2 F cm ^{–3}	4.83 mWh cm ^{–3}	–	[139]
	SCs/MXene	–	PVA/H ₂ SO ₄	0–0.6	–	2.1 F cm ^{–2}	0.0244 mWh cm ^{–3}	–	[136]
Flexographic printing	Zn–MnO ₂ batteries	PSBR	Zn ⁺ Tf [–] in BMIM ⁺ Tf [–] , PVDF–HFP	0.5–1.8	28	0.16 mAh cm ^{–2}	–	–	[81]
Transfer printing	LIBs/Li–LCO	–	LiPON	3–4.2	2.9–3.8	0.106 mAh cm ^{–2}	–	Bendable, integration	[143]
	SCs/MXene	–	PVA/H ₂ SO ₄	0–0.6	0.69	61 mF cm ^{–2}	0.76 $\mu\text{Wh cm}^{-2}$	Customized shapes	[84]

FEC—fluoroethylene carbonate, DMC—dimethyl carbonate, SDBS—sodium dodecylbenzene sulfonate, SBN—sebaconitrile, P-VC/VAc—poly(vinyl chloride-co-vinyl acetate), EC—ethylene carbonate, DEC—diethyl carbonate, DMSO—dimethyl sulfoxide, BMIM⁺Tf[–]—1-butyl-3-methylimidazolium trifluoromethanesulfonate, PAA—polyacrylic acid, TMPPT—trimethylolpropane tris(3-mercaptopropionate), TMPTA—trimethylolpropane triacrylate, LiTFSI—lithium bis(trifluoromethylsulfonyl)imide; EMIMTFSI—1-ethyl-3-methylimidazolium bis(trifluoromethylsulfonyl)imide

energy from ambient environment or human motion into electricity, storage in EESDs and usage in electronics as needed (e.g., sensors) is the ultimate pursuit to satisfy the energy requirements of these maintenance-free electronics [180, 181]. And although some prototypes have been demonstrated [165, 167], many unresolved issues remain, including mismatching between energy harvesters and EESDs, low energy conversion efficiency and poor compatibility between the preparation processes of energy harvesters and printable EESDs, all of which require optimizations in circuit design and comprehensive considerations in different technical processes [182].

Lastly, a unified evaluation standard in device performance and functionality has yet to be established for EESDs, resulting in huge difficulties while comparing printable EESDs from different publications [73]. However, appropriate standards are the premise of actual applications, especially for reliability and functionality. In the future, security tests (e.g., puncture, cutting, fireproofing tests) should be carried out during in all charge–discharge depth rather than in static states and functionality tests (e.g.,

bending, twisting, stretching tests) should be conducted during dynamic discharging processes, to more closely simulate actual situations.

Overall, wearable and smart electronics are becoming increasingly integrated into everyday life and due to prominent advantages of cost, efficiency, scalability, design ability and customization, printable EESDs are highly competitive candidates as the power source of these flexible and wearable electronics that require diverse form factors. And although great progress has been made in the performance and form factors of printable EESDs, the actual application of printable EESDs remains challenging. These challenges including: (1) most raw materials used in the preparation of electrode inks are nanomaterials, the low-cost and controllable production of which have yet to be fully realized [183]; (2) the seamless integration of printable EESDs with printable energy consumption electronics has yet to be demonstrated with acceptable performances even if their fabrication techniques are similar; and (3) most achievements reported are at the laboratory level and cannot be extended to the scalable production of printable EESDs with multiple

form factors if simultaneously considering the technical processes, costs, safety, performances and target applications. As a result, continuous effort and multidisciplinary cooperation are necessary. Despite this, there is no doubt that printed power sources will become increasingly pervasive and will gradually be integrated into almost every aspect of everyday life.

Acknowledgements This work was financially supported by the National Natural Science Foundation of China (Grants 51872283, 21805273), the National Key R&D Program of China (Grants 2016YFB0100100, 2016YFA0200200), the Liaoning Revitalization Talents Program (Grant XLYC1807153), Liaoning BaiQianWan Talents Program, the Natural Science Foundation of Liaoning Province, the Joint Research Fund Liaoning-Shenyang National Laboratory for Materials Science (Grant 20180510038), DICP (DICP ZZBS201708, DICP ZZBS201802), DICP&QIBEBT (Grant DICP&QIBEBT UN201702), the DNL Cooperation Fund, CAS (DNL180310, DNL180308, DNL201912 and DNL201915).

References

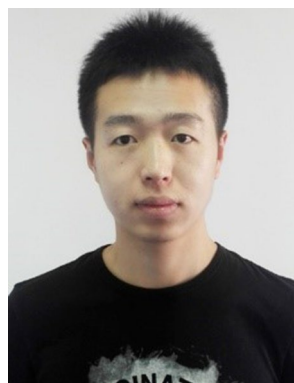
- Zhang, C., Lv, W., Tao, Y., et al.: Towards superior volumetric performance: design and preparation of novel carbon materials for energy storage. *Energy Environ. Sci.* **8**, 1390–1403 (2015)
- Kyeremateng, N.A., Brousse, T., Pech, D.: Microsupercapacitors as miniaturized energy-storage components for on-chip electronics. *Nat. Nanotechnol.* **12**, 7–15 (2017)
- Lin, D., Liu, Y., Cui, Y.: Reviving the lithium metal anode for high-energy batteries. *Nat. Nanotechnol.* **12**, 194–206 (2017)
- Fang, R., Zhao, S., Sun, Z., et al.: More reliable lithium–sulfur batteries: status, solutions and prospects. *Adv. Mater.* **29**, 1606823 (2017)
- Fang, R., Chen, K., Yin, L., et al.: The regulating role of carbon nanotubes and graphene in lithium-ion and lithium–sulfur batteries. *Adv. Mater.* **31**, 1800863 (2019)
- Dong, Y., Wu, Z.-S., Ren, W., et al.: Graphene: a promising 2D material for electrochemical energy storage. *Sci. Bull.* **62**, 724–740 (2017)
- Zhang, J., Zhang, G., Zhou, T., et al.: Recent developments of planar micro-supercapacitors: fabrication, properties, and applications. *Adv. Funct. Mater.* **30**, 1910000 (2020)
- Wen, L., Li, F., Cheng, H.M.: Carbon nanotubes and graphene for flexible electrochemical energy storage: from materials to devices. *Adv. Mater.* **28**, 4306–4337 (2016)
- Liu, W., Song, M.S., Kong, B., et al.: Flexible and stretchable energy storage: recent advances and future perspectives. *Adv. Mater.* **29**, 1603436 (2017)
- Dubal, D.P., Chodankar, N.R., Kim, D.H., et al.: Towards flexible solid-state supercapacitors for smart and wearable electronics. *Chem. Soc. Rev.* **47**, 2065–2129 (2018)
- Li, L., Lou, Z., Chen, D., et al.: Recent advances in flexible/stretchable supercapacitors for wearable electronics. *Small* **14**, 1702829 (2018)
- Zhang, H., Liao, X., Guan, Y., et al.: Lithiophilic–lithiophobic gradient interfacial layer for a highly stable lithium metal anode. *Nat. Commun.* **9**, 3729 (2018)
- Xue, P., Liu, S., Shi, X., et al.: A hierarchical silver-nanowire-graphene host enabling ultrahigh rates and superior long-term cycling of lithium-metal composite anodes. *Adv. Mater.* **30**, 1804165 (2018)
- Zhang, Y., Song, Q., Wang, T., et al.: Crystal preferred orientation of $\text{Li}_2\text{MnO}_3\text{-LiMO}_2$ ($M = \text{Mn Co, Ni}$) nano-particles: relevance to electrochemical behavior for lithium battery cathode materials. *J. Power Sources* **413**, 425–431 (2019)
- Wu, Z.S., Tan, Y.Z., Zheng, S., et al.: Bottom-up fabrication of sulfur-doped graphene films derived from sulfur-annulated nanographene for ultrahigh volumetric capacitance micro-supercapacitors. *J. Am. Chem. Soc.* **139**, 4506–4512 (2017)
- Lukatskaya, M.R., Kota, S., Lin, Z., et al.: Ultra-high-rate pseudocapacitive energy storage in two-dimensional transition metal carbides. *Nat. Energy* **2**, 17105 (2017)
- Suo, L., Borodin, O., Gao, T., et al.: “Water-in-salt” electrolyte enables high-voltage aqueous lithium-ion chemistries. *Science* **350**, 938–943 (2015)
- Dou, Q., Lei, S., Wang, D.W., et al.: Safe and high-rate supercapacitors based on an “acetonitrile/water in salt” hybrid electrolyte. *Energy Environ. Sci.* **11**, 3212–3219 (2018)
- Dou, Q., Liu, L., Yang, B., et al.: Silica-grafted ionic liquids for revealing the respective charging behaviors of cations and anions in supercapacitors. *Nat. Commun.* **8**, 2188 (2017)
- Zheng, S., Zhang, C., Zhou, F., et al.: Ionic liquid pre-intercalated MXene films for ionogel-based flexible micro-supercapacitors with high volumetric energy density. *J. Mater. Chem. A* **7**, 9478–9485 (2019)
- Fan, L., Wei, S., Li, S., et al.: Recent progress of the solid-state electrolytes for high-energy metal-based batteries. *Adv. Energy Mater.* **8**, 1702657 (2018)
- Fan, X., Yue, J., Han, F., et al.: High-performance all-solid-state Na–S battery enabled by casting–annealing technology. *ACS Nano* **12**, 3360–3368 (2018)
- Li, X., Liang, J., Li, X., et al.: High-performance all-solid-state Li–Se batteries induced by sulfide electrolytes. *Energy Environ. Sci.* **11**, 2828–2832 (2018)
- Zheng, S., Shi, X., Das, P., et al.: The road towards planar microbatteries and micro-supercapacitors: from 2D to 3D device geometries. *Adv. Mater.* **31**, 1900583 (2019)
- Pech, D., Brunet, M., Durou, H., et al.: Ultrahigh-power micro-metre-sized supercapacitors based on onion-like carbon. *Nat. Nanotechnol.* **5**, 651–654 (2010)
- Lin, J., Zhang, C., Yan, Z., et al.: 3-Dimensional graphene carbon nanotube carpet-based microsupercapacitors with high electrochemical performance. *Nano Lett.* **13**, 72–78 (2013)
- Liang, Y., Jing, Y., Gheytani, S., et al.: Universal quinone electrodes for long cycle life aqueous rechargeable batteries. *Nat. Mater.* **16**, 841–848 (2017)
- Zeng, Y., Zhang, X., Meng, Y., et al.: Achieving ultrahigh energy density and long durability in a flexible rechargeable quasi-solid-state Zn– MnO_2 battery. *Adv. Mater.* **29**, 1700274 (2017)
- Pang, Q., Shyamsunder, A., Narayanan, B., et al.: Tuning the electrolyte network structure to invoke quasi-solid state sulfur conversion and suppress lithium dendrite formation in Li–S batteries. *Nat. Energy* **3**, 783–791 (2018)
- Fang, R., Li, G., Zhao, S., et al.: Single-wall carbon nanotube network enabled ultrahigh sulfur-content electrodes for high-performance lithium–sulfur batteries. *Nano Energy* **42**, 205–214 (2017)
- Yang, X., Li, X., Adair, K., et al.: Structural design of lithium–sulfur batteries: from fundamental research to practical application. *Electrochem. Energy Rev.* **1**, 239–293 (2018)
- Li, Y.J., Cui, L., Da, P.F., et al.: Multiscale structural engineering of Ni-doped CoO nanosheets for zinc-air batteries with high power density. *Adv. Mater.* **30**, 1804653 (2018)
- Zhang, Y., Ding, J., Qi, B., et al.: Multifunctional fibers to shape future biomedical devices. *Adv. Funct. Mater.* **29**, 1902834 (2019)

34. Pan, S., Ren, J., Fang, X., et al.: Integration: an effective strategy to develop multifunctional energy storage devices. *Adv. Energy Mater.* **6**, 1501867 (2016)
35. Shi, X., Zheng, S., Wu, Z.S., et al.: Recent advances of graphene-based materials for high-performance and new-concept supercapacitors. *J. Energy Chem.* **27**, 25–42 (2018)
36. Choi, K.H., Ahn, D.B., Lee, S.Y.: Current status and challenges in printed batteries: toward form factor-free, monolithic integrated power sources. *ACS Energy Lett.* **3**, 220–236 (2018)
37. Dinh, T.M., Armstrong, K., Guay, D., et al.: High-resolution on-chip supercapacitors with ultra-high scan rate ability. *J. Mater. Chem. A* **2**, 7170–7174 (2014)
38. Shen, C., Wang, X., Li, S., et al.: A high-energy-density micro supercapacitor of asymmetric MnO₂–carbon configuration by using micro-fabrication technologies. *J. Power Sources* **234**, 302–309 (2013)
39. Chmiola, J., Largeot, C., Taberna, P.L., et al.: Monolithic carbide-derived carbon films for micro-supercapacitors. *Science* **328**, 480–483 (2010)
40. Wu, Z.S., Parvez, K., Feng, X., et al.: Graphene-based in-plane micro-supercapacitors with high power and energy densities. *Nat. Commun.* **4**, 2487 (2013)
41. Wu, Z.S., Parvez, K., Feng, X., et al.: Photolithographic fabrication of high-performance all-solid-state graphene-based planar micro-supercapacitors with different interdigital fingers. *J. Mater. Chem. A* **2**, 8288–8293 (2014)
42. Wu, Z.S., Yang, S., Zhang, L., et al.: Binder-free activated graphene compact films for all-solid-state micro-supercapacitors with high areal and volumetric capacitances. *Energy Storage Mater.* **1**, 119–126 (2015)
43. Wu, Z.S., Zheng, Y., Zheng, S., et al.: Stacked-layer heterostructure films of 2D thiophene nanosheets and graphene for high-rate all-solid-state pseudocapacitors with enhanced volumetric capacitance. *Adv. Mater.* **29**, 1602960 (2017)
44. Gao, W., Singh, N., Song, L., et al.: Direct laser writing of micro-supercapacitors on hydrated graphite oxide films. *Nat. Nanotechnol.* **6**, 496–500 (2011)
45. El-Kady, M.F., Kaner, R.B.: Scalable fabrication of high-power graphene micro-supercapacitors for flexible and on-chip energy storage. *Nat. Commun.* **4**, 1475 (2013)
46. Lin, J., Peng, Z., Liu, Y., et al.: Laser-induced porous graphene films from commercial polymers. *Nat. Commun.* **5**, 5714 (2014)
47. El-Kady, M.F., Ihms, M., Li, M., et al.: Engineering three-dimensional hybrid supercapacitors and microsupercapacitors for high-performance integrated energy storage. *Proc. Natl. Acad. Sci. U. S. A.* **112**, 4233–4238 (2015)
48. Liu, W.W., Feng, Y.Q., Yan, X.-B., et al.: Superior micro-supercapacitors based on graphene quantum dots. *Adv. Funct. Mater.* **23**, 4111–4122 (2013)
49. Xiao, H., Wu, Z.S., Chen, L., et al.: One-step device fabrication of phosphorene and graphene interdigital micro-supercapacitors with high energy density. *ACS Nano* **11**, 7284–7292 (2017)
50. Zhou, F., Huang, H., Xiao, C., et al.: Electrochemically scalable production of fluorine-modified graphene for flexible and high-energy ionogel-based microsupercapacitors. *J. Am. Chem. Soc.* **140**, 8198–8205 (2018)
51. Tian, H., Qin, J., Hou, D., et al.: General interfacial self-assembly engineering for patterning two-dimensional polymers with cylindrical mesopores on graphene. *Angew. Chem. Int. Ed.* **58**, 10173–10178 (2019)
52. Wang, S., Wu, Z.S., Zheng, S., et al.: Scalable fabrication of photochemically reduced graphene-based monolithic micro-supercapacitors with superior energy and power densities. *ACS Nano* **11**, 4283–4291 (2017)
53. Peng, Y.Y., Akuzum, B., Kurra, N., et al.: All-MXene (2D titanium carbide) solid-state microsupercapacitors for on-chip energy storage. *Energy Environ. Sci.* **9**, 2847–2854 (2016)
54. Gaikwad, A.M., Arias, A.C., Steingart, D.A.: Recent progress on printed flexible batteries: mechanical challenges, printing technologies, and future prospects. *Energy Technol.* **3**, 305–328 (2015)
55. Lin, Y., Gao, Y., Fang, F., et al.: Recent progress on printable power supply devices and systems with nanomaterials. *Nano Res.* **11**, 3065–3087 (2018)
56. Li, H., Liang, J.: Recent development of printed micro-supercapacitors: printable materials, printing technologies, and perspectives. *Adv. Mater.* **31**, 1805864 (2019)
57. Zhang, Y.Z., Wang, Y., Cheng, T., et al.: Printed supercapacitors: materials, printing and applications. *Chem. Soc. Rev.* **48**, 3229–3264 (2019)
58. Pang, Y., Cao, Y., Chu, Y., et al.: Additive manufacturing of batteries. *Adv. Funct. Mater.* **30**, 1906244 (2019)
59. Hu, G., Kang, J., Ng, L.W.T., et al.: Functional inks and printing of two-dimensional materials. *Chem. Soc. Rev.* **47**, 3265–3300 (2018)
60. Azzellino, G., Grimoldi, A., Binda, M., et al.: Fully inkjet-printed organic photodetectors with high quantum yield. *Adv. Mater.* **25**, 6829–6833 (2013)
61. Ota, H., Chao, M., Gao, Y., et al.: 3D printed “earable” smart devices for real-time detection of core body temperature. *ACS Sens.* **2**, 990–997 (2017)
62. Dua, V., Surwade, S.P., Ammu, S., et al.: All-organic vapor sensor using inkjet-printed reduced graphene oxide. *Angew. Chem. Int. Ed.* **49**, 2154–2157 (2010)
63. Torrisi, F., Hasan, T., Wu, W., et al.: Inkjet-printed graphene electronics. *ACS Nano* **6**, 2992–3006 (2012)
64. Singh, N., Galande, C., Miranda, A., et al.: Paintable battery. *Sci. Rep.* **2**, 481 (2012)
65. Gao, X., Dong, Y., Li, S., et al.: MOFs and COFs for batteries and supercapacitors. *Electrochem. Energy Rev.* **3**, 81–126 (2019)
66. Zhou, G., Li, F., Cheng, H.-M.: Progress in flexible lithium batteries and future prospects. *Energy Environ. Sci.* **7**, 1307–1338 (2014)
67. Xue, W., Shi, Z., Suo, L., et al.: Intercalation-conversion hybrid cathodes enabling Li–S full-cell architectures with jointly superior gravimetric and volumetric energy densities. *Nat. Energy* **4**, 374–382 (2019)
68. Yang, C., Chen, J., Ji, X., et al.: Aqueous Li-ion battery enabled by halogen conversion–intercalation chemistry in graphite. *Nature* **569**, 245–250 (2019)
69. Beidaghi, M., Gogotsi, Y.: Capacitive energy storage in micro-scale devices: recent advances in design and fabrication of micro-supercapacitors. *Energy Environ. Sci.* **7**, 867–884 (2014)
70. Zheng, S., Wu, Z.S., Wang, S., et al.: Graphene-based materials for high-voltage and high-energy asymmetric supercapacitors. *Energy Storage Mater.* **6**, 70–97 (2017)
71. Vlad, A., Singh, N., Galande, C., et al.: Design considerations for unconventional electrochemical energy storage architectures. *Adv. Energy Mater.* **5**, 1402115 (2015)
72. Liu, L., Niu, Z., Chen, J.: Unconventional supercapacitors from nanocarbon-based electrode materials to device configurations. *Chem. Soc. Rev.* **45**, 4340–4363 (2016)
73. Du, C.F., Liang, Q., Luo, Y., et al.: Recent advances in printable secondary batteries. *J. Mater. Chem. A* **5**, 22442–22458 (2017)
74. Zheng, S., Tang, X., Wu, Z.-S., et al.: Arbitrary-shaped graphene-based planar sandwich supercapacitors on one substrate with enhanced flexibility and integration. *ACS Nano* **11**, 2171–2179 (2017)

75. Choi, K.H., Yoo, J., Lee, C.K., et al.: All-inkjet-printed, solid-state flexible supercapacitors on paper. *Energy Environ. Sci.* **9**, 2812–2821 (2016)
76. Sundriyal, P., Bhattacharya, S.: Inkjet-printed electrodes on A4 paper substrates for low-cost, disposable, and flexible asymmetric supercapacitors. *ACS Appl. Mater. Interfaces* **9**, 38507–38521 (2017)
77. Kim, S.H., Choi, K.H., Cho, S.J., et al.: Flexible/shape-versatile, bipolar all-solid-state lithium-ion batteries prepared by multi-stage printing. *Energy Environ. Sci.* **11**, 321–330 (2018)
78. Kumar, R., Shin, J., Yin, L., et al.: All-printed, stretchable Zn–Ag₂O rechargeable battery via hyperelastic binder for self-powering wearable electronics. *Adv. Energy Mater.* **7**, 1602096 (2017)
79. Shi, X., Pei, S., Zhou, F., et al.: Ultrahigh-voltage integrated micro-supercapacitors with designable shapes and superior flexibility. *Energy Environ. Sci.* **12**, 1534–1541 (2019)
80. Yao, B., Chandrasekaran, S., Zhang, J., et al.: Efficient 3D printed pseudocapacitive electrodes with ultrahigh MnO₂ loading. *Joule* **3**, 1–12 (2019)
81. Wang, Z., Winslow, R., Madan, D., et al.: Development of MnO₂ cathode inks for flexographically printed rechargeable zinc-based battery. *J. Power Sources* **268**, 246–254 (2014)
82. Secor, E.B., Lim, S., Zhang, H., et al.: Gravure printing of graphene for large-area flexible electronics. *Adv. Mater.* **26**, 4533–4538 (2014)
83. Jiang, Q., Kurra, N., Alshareef, H.N.: Marker pen lithography for flexible and curvilinear on-chip energy storage. *Adv. Funct. Mater.* **25**, 4976–4984 (2015)
84. Zhang, C.J., Kremer, M.P., Seral-Ascaso, A., et al.: Stamping of flexible, coplanar micro-supercapacitors using MXene inks. *Adv. Funct. Mater.* **28**, 1705506 (2018)
85. Shi, X., Wu, Z.S., Qin, J., et al.: Graphene-based linear tandem micro-supercapacitors with metal-free current collectors and high-voltage output. *Adv. Mater.* **29**, 1703034 (2017)
86. Wang, X., Lu, Q., Chen, C., et al.: A consecutive spray printing strategy to construct and integrate diverse supercapacitors on various substrates. *ACS Appl. Mater. Interfaces* **9**, 28612–28619 (2017)
87. Niu, S., Lv, W., Zhou, G., et al.: Electrostatic-spraying an ultrathin, multifunctional and compact coating onto a cathode for a long-life and high-rate lithium-sulfur battery. *Nano Energy* **30**, 138–145 (2016)
88. Zheng, S., Lei, W., Qin, J., et al.: All-solid-state high-energy planar asymmetric supercapacitors based on all-in-one monolithic film using boron nitride nanosheets as separator. *Energy Storage Mater.* **10**, 24–31 (2018)
89. Wu, Z.S., Liu, Z., Parvez, K., et al.: Ultrathin printable graphene supercapacitors with AC line-filtering performance. *Adv. Mater.* **27**, 3669–3675 (2015)
90. Liu, Z., Wu, Z.S., Yang, S., et al.: Ultraflexible in-plane micro-supercapacitors by direct printing of solution-processable electrochemically exfoliated graphene. *Adv. Mater.* **28**, 2217–2222 (2016)
91. Sekitani, T., Noguchi, Y., Zschieschang, U., et al.: Organic transistors manufactured using inkjet technology with subfemtoliter accuracy. *Proc. Natl. Acad. Sci. U. S. A.* **105**, 4976–4980 (2008)
92. Zhang, Y., Anderson, N., Bland, S., et al.: All-printed strain sensors: building blocks of the aircraft structural health monitoring system. *Sens. Actuators A Phys.* **253**, 165–172 (2017)
93. Delannoy, P.E., Riou, B., Brousse, T., et al.: Ink-jet printed porous composite LiFePO₄ electrode from aqueous suspension for microbatteries. *J. Power Sources* **287**, 261–268 (2015)
94. Zhao, Y., Zhou, Q., Liu, L., et al.: A novel and facile route of ink-jet printing to thin film SnO₂ anode for rechargeable lithium ion batteries. *Electrochim. Acta* **51**, 2639–2645 (2006)
95. Lawes, S., Sun, Q., Lushington, A., et al.: Inkjet-printed silicon as high performance anodes for Li-ion batteries. *Nano Energy* **36**, 313–321 (2017)
96. Chen, P., Chen, H., Qiu, J., et al.: Inkjet printing of single-walled carbon nanotube/RuO₂ nanowire supercapacitors on cloth fabrics and flexible substrates. *Nano Res.* **3**, 594–603 (2010)
97. Cheng, T., Zhang, Y.Z., Yi, J.P., et al.: Inkjet-printed flexible, transparent and aesthetic energy storage devices based on PEDOT:PSS/Ag grid electrodes. *J. Mater. Chem. A* **4**, 13754–13763 (2016)
98. Pech, D., Brunet, M., Taberna, P.L., et al.: Elaboration of a microstructured inkjet-printed carbon electrochemical capacitor. *J. Power Sources* **195**, 1266–1269 (2010)
99. Pei, Z., Hu, H., Liang, G., et al.: Carbon-based flexible and all-solid-state micro-supercapacitors fabricated by inkjet printing with enhanced performance. *Nano-Micro Lett.* **9**, 9–19 (2017)
100. Liu, W., Lu, C., Li, H., et al.: Paper-based all-solid-state flexible micro-supercapacitors with ultra-high rate and rapid frequency response capabilities. *J. Mater. Chem. A* **4**, 3754–3764 (2016)
101. Li, J., Ye, F., Vaziri, S., et al.: Efficient inkjet printing of graphene. *Adv. Mater.* **25**, 3985–3992 (2013)
102. Hu, L., Cui, Y.: Energy and environmental nanotechnology in conductive paper and textiles. *Energy Environ. Sci.* **5**, 6423 (2012)
103. Anasori, B., Lukatskaya, M.R., Gogotsi, Y.: 2D metal carbides and nitrides (MXenes) for energy storage. *Nat. Rev. Mater.* **2**, 16098 (2017)
104. Zhong, J., Sun, W., Wei, Q., et al.: Efficient and scalable synthesis of highly aligned and compact two-dimensional nanosheet films with record performances. *Nat. Commun.* **9**, 3484 (2018)
105. Zhang, C.J., Mckeon, L., Kremer, M.P., et al.: Additive-free MXene inks and direct printing of micro-supercapacitors. *Nat. Commun.* **10**, 1795 (2019)
106. Jost, K., Stenger, D., Perez, C.R., et al.: Knitted and screen printed carbon-fiber supercapacitors for applications in wearable electronics. *Energy Environ. Sci.* **6**, 2698–2705 (2013)
107. Abdelkader, A.M., Karim, N., Vallés, C., et al.: Ultraflexible and robust graphene supercapacitors printed on textiles for wearable electronics applications. *2D Mater.* **4**, 035016 (2017)
108. Liu, S., Xie, J., Li, H., et al.: Nitrogen-doped reduced graphene oxide for high-performance flexible all-solid-state micro-supercapacitors. *J. Mater. Chem. A* **2**, 18125–18131 (2014)
109. Liu, L., Tian, Q., Yao, W., et al.: All-printed ultraflexible and stretchable asymmetric in-plane solid-state supercapacitors (ASCs) for wearable electronics. *J. Power Sources* **397**, 59–67 (2018)
110. Li, H., Liu, S., Li, X., et al.: Screen-printing fabrication of high volumetric energy density micro-supercapacitors based on high-resolution thixotropic-ternary hybrid interdigital micro-electrodes. *Mater. Chem. Front.* **3**, 626–635 (2019)
111. Li, J., Sollami Deleka, S., Zhang, P., et al.: Scalable fabrication and integration of graphene microsupercapacitors through full inkjet printing. *ACS Nano* **11**, 8249–8256 (2017)
112. Kim, S.H., Choi, K.H., Cho, S.J., et al.: Printable solid-state lithium-ion batteries: a new route toward shape-conformable power sources with aesthetic versatility for flexible electronics. *Nano Lett.* **15**, 5168–5177 (2015)

113. Braam, K., Subramanian, V.: A stencil printed, high energy density silver oxide battery using a novel photopolymerizable poly(acrylic acid) separator. *Adv. Mater.* **27**, 689–694 (2015)
114. Zhu, C., Liu, T., Qian, F., et al.: 3D printed functional nanomaterials for electrochemical energy storage. *Nano Today* **15**, 107–120 (2017)
115. Zhang, F., Wei, M., Viswanathan, V.V., et al.: 3D printing technologies for electrochemical energy storage. *Nano Energy* **40**, 418–431 (2017)
116. Zhu, C., Liu, T., Qian, F., et al.: Supercapacitors based on three-dimensional hierarchical graphene aerogels with periodic macropores. *Nano Lett.* **16**, 3448–3456 (2016)
117. Sun, K., Wei, T.S., Ahn, B.Y., et al.: 3D printing of interdigitated Li-ion microbattery architectures. *Adv. Mater.* **25**, 4539–4543 (2013)
118. Fu, K., Wang, Y., Yan, C., et al.: Graphene oxide-based electrode inks for 3D-printed lithium-ion batteries. *Adv. Mater.* **28**, 2587–2594 (2016)
119. Blake, A.J., Kohlmeyer, R.R., Hardin, J.O., et al.: 3D printable ceramic-polymer electrolytes for flexible high-performance Li-ion batteries with enhanced thermal stability. *Adv. Energy Mater.* **7**, 1602920 (2017)
120. Wei, T.S., Ahn, B.Y., Grotto, J., et al.: 3D printing of customized Li-ion batteries with thick electrodes. *Adv. Mater.* **30**, 1703027 (2018)
121. Hu, J., Jiang, Y., Cui, S., et al.: 3D-printed cathodes of $\text{LiMn}_{1-x}\text{Fe}_x\text{PO}_4$ nanocrystals achieve both ultrahigh rate and high capacity for advanced lithium-ion battery. *Adv. Energy Mater.* **6**, 1600856 (2016)
122. Ho, C.C., Evans, J.W., Wright, P.K.: Direct write dispenser printing of a zinc microbattery with an ionic liquid gel electrolyte. *J. Micromech. Microeng.* **20**, 104009 (2010)
123. Cao, D., Xing, Y., Tantratian, K., et al.: 3D printed high-performance lithium metal microbatteries enabled by nanocellulose. *Adv. Mater.* **31**, 1807313 (2019)
124. Lyu, Z., Lim, G.J.H., Guo, R., et al.: 3D-printed electrodes for lithium metal batteries with high areal capacity and high-rate capability. *Energy Storage Mater.* **24**, 336–342 (2020)
125. Gao, X., Yang, X., Sun, Q., et al.: Converting a thick electrode into vertically aligned “Thin electrodes” by 3D-printing for designing thickness independent Li-S cathode. *Energy Storage Mater.* **24**, 682–688 (2020)
126. Lacey, S.D., Kirsch, D.J., Li, Y., et al.: Extrusion-based 3D printing of hierarchically porous advanced battery electrodes. *Adv. Mater.* **30**, 1705651 (2018)
127. Garcia-Tunon, E., Barg, S., Franco, J., et al.: Printing in three dimensions with graphene. *Adv. Mater.* **27**, 1688–1693 (2015)
128. Wei, X., Li, D., Jiang, W., et al.: 3D printable graphene composite. *Sci. Rep.* **5**, 11181 (2015)
129. Zhu, C., Han, T.Y., Duoss, E.B., et al.: Highly compressible 3D periodic graphene aerogel microlattices. *Nat. Commun.* **6**, 6962 (2015)
130. Zhang, D., Chi, B., Li, B., et al.: Fabrication of highly conductive graphene flexible circuits by 3D printing. *Synth. Met.* **217**, 79–86 (2016)
131. Zhang, Q., Zhang, F., Medarametla, S.P., et al.: 3D printing of graphene aerogels. *Small* **12**, 1702–1708 (2016)
132. Lin, Y., Liu, F., Casano, G., et al.: Pristine graphene aerogels by room-temperature freeze gelation. *Adv. Mater.* **28**, 7993–8000 (2016)
133. Jiang, Y., Xu, Z., Huang, T., et al.: Direct 3D printing of ultralight graphene oxide aerogel microlattices. *Adv. Funct. Mater.* **28**, 1707024 (2018)
134. Wang, Z., Zhang, Q.E., Long, S., et al.: Three-dimensional printing of polyaniline/reduced graphene oxide composite for high-performance planar supercapacitor. *ACS Appl. Mater. Interfaces* **10**, 10437–10444 (2018)
135. Rocha, V.G., Garcia-Tunon, E., Botas, C., et al.: Multimaterial 3D printing of graphene-based electrodes for electrochemical energy storage using thermoresponsive inks. *ACS Appl. Mater. Interfaces* **9**, 37136–37145 (2017)
136. Yang, W., Yang, J., Byun, J.J., et al.: 3D printing of freestanding MXene architectures for current-collector-free supercapacitors. *Adv. Mater.* **31**, 1902725 (2019)
137. Yu, L., Fan, Z., Shao, Y., et al.: Versatile N-doped MXene ink for printed electrochemical energy storage application. *Adv. Energy Mater.* **9**, 1901839 (2019)
138. Zhang, C.J., Anasori, B., Seral-Ascaso, A., et al.: Transparent, flexible, and conductive 2D titanium carbide (MXene) films with high volumetric capacitance. *Adv. Mater.* **29**, 1702678 (2017)
139. Liu, Y., Zhang, B., Xu, Q., et al.: Development of graphene oxide/polyaniline inks for high performance flexible microsupercapacitors via extrusion printing. *Adv. Funct. Mater.* **28**, 1706592 (2018)
140. Zhao, C., Wang, C., Gorkin, R., et al.: Three dimensional (3D) printed electrodes for interdigitated supercapacitors. *Electrochem. Commun.* **41**, 20–23 (2014)
141. Xiao, Y., Huang, L., Zhang, Q., et al.: Gravure printing of hybrid MoS_2 @S-rGO interdigitated electrodes for flexible microsupercapacitors. *Appl. Phys. Lett.* **107**, 10756 (2015)
142. Meitl, M.A., Zhu, Z., Kumar, V., et al.: Transfer printing by kinetic control of adhesion to an elastomeric stamp. *Nat. Mater.* **5**, 33–38 (2006)
143. Koo, M., Park, K.I., Lee, S.H., et al.: Bendable inorganic thin-film battery for fully flexible electronic systems. *Nano Lett.* **12**, 4810–4816 (2012)
144. Li, Z., Liu, H., Ouyang, C., et al.: Recent advances in pen-based writing electronics and their emerging applications. *Adv. Funct. Mater.* **26**, 165–180 (2016)
145. Bandonkar, A.J., Jia, W., Ramirez, J., et al.: Biocompatible enzymatic roller pens for direct writing of biocatalytic materials: “Do-it-Yourself” electrochemical biosensors. *Adv. Healthc. Mater.* **4**, 1215–1224 (2015)
146. Qi, Z., Zhang, F., Di, C.A., et al.: All-brush-painted top-gate organic thin-film transistors. *J. Mater. Chem. C* **1**, 3072 (2013)
147. Fu, Y., Cai, X., Wu, H., et al.: Fiber supercapacitors utilizing pen ink for flexible/wearable energy storage. *Adv. Mater.* **24**, 5713–5718 (2012)
148. Quain, E., Mathis, T.S., Kurra, N., et al.: Direct writing of additive-free MXene-in-water ink for electronics and energy storage. *Adv. Mater. Technol.* **4**, 1800256 (2019)
149. Guo, K., Wan, Y., Yu, N., et al.: Hand-drawing patterned ultrathin integrated electrodes for flexible micro supercapacitors. *Energy Storage Mater.* **11**, 144–151 (2018)
150. Zhu, M., Huang, Y., Huang, Y., et al.: A highly durable, transferable, and substrate-versatile high-performance all-polymer micro-supercapacitor with plug-and-play function. *Adv. Mater.* **29**, 1605137 (2017)
151. Lee, S.S., Choi, K.H., Kim, S.H., et al.: Wearable supercapacitors printed on garments. *Adv. Funct. Mater.* **28**, 1705571 (2018)
152. Shi, Y., Wang, Y., Gu, Y., et al.: Self-healable and stretchable ionogels serve as electrolytes and substrates for integrated all-in-one micro-supercapacitors. *Chem. Eng. J.* **392**, 123645 (2019)

153. Kim, D., Shin, G., Kang, Y.J., et al.: Fabrication of a stretchable solid-state micro-supercapacitor array. *ACS Nano* **7**, 7975–7982 (2013)
154. Xie, H., Bao, Y., Cheng, J., et al.: Flexible garnet solid-state electrolyte membranes enabled by tile-and-grout design. *ACS Energy Lett.* **4**, 2668–2674 (2019)
155. Wang, X., Zheng, S., Zhou, F., et al.: Scalable fabrication of printed Zn/MnO₂ planar micro-batteries with high volumetric energy density and exceptional safety. *Natl Sci. Rev.* **6**, 1–9 (2020)
156. Thekkekara, L.V., Gu, M.: Bioinspired fractal electrodes for solar energy storages. *Sci. Rep.* **7**, 45585 (2017)
157. Laszczyk, K.U., Kobashi, K., Sakurai, S., et al.: Lithographically integrated microsupercapacitors for compact, high performance, and designable energy circuits. *Adv. Energy Mater.* **5**, 1500741 (2015)
158. Sun, H., Fu, X., Xie, S., et al.: Electrochemical capacitors with high output voltages that mimic electric eels. *Adv. Mater.* **28**, 2070–2076 (2016)
159. Wu, Z.S., Parvez, K., Li, S., et al.: Alternating stacked graphene-conducting polymer compact films with ultrahigh areal and volumetric capacitances for high-energy micro-supercapacitors. *Adv. Mater.* **27**, 4054–4061 (2015)
160. Lu, Y., Jiang, K., Chen, D., et al.: Wearable sweat monitoring system with integrated micro-supercapacitors. *Nano Energy* **58**, 624–632 (2019)
161. Niu, S., Matsuhisa, N., Beker, L., et al.: A wireless body area sensor network based on stretchable passive tags. *Nat. Electron.* **2**, 361–368 (2019)
162. Wen, Z., Yeh, M.H., Guo, H., et al.: Self-powered textile for wearable electronics by hybridizing fiber-shaped nanogenerators, solar cells, and supercapacitors. *Sci. Adv.* **2**, e1600097 (2016)
163. Qin, S., Zhang, Q., Yang, X., et al.: Hybrid piezo/triboelectric-driven self-charging electrochromic supercapacitor power package. *Adv. Energy Mater.* **8**, 1800069 (2018)
164. Yun, J., Song, C., Lee, H., et al.: Stretchable array of high-performance micro-supercapacitors charged with solar cells for wireless powering of an integrated strain sensor. *Nano Energy* **49**, 644–654 (2018)
165. Lin, Y., Chen, J., Tavakoli, M.M., et al.: Printable fabrication of a fully integrated and self-powered sensor system on plastic substrates. *Adv. Mater.* **31**, 1804285 (2019)
166. Xu, S., Dall'agnese, Y., Wei, G., et al.: Screen-printable micro-scale hybrid device based on MXene and layered double hydroxide electrodes for powering force sensors. *Nano Energy* **50**, 479–488 (2018)
167. Um, H.D., Choi, K.H., Hwang, I., et al.: Monolithically integrated, photo-rechargeable portable power sources based on miniaturized Si solar cells and printed solid-state lithium-ion batteries. *Energy Environ. Sci.* **10**, 931–940 (2017)
168. Zhu, M., Wang, Z., Li, H., et al.: Light-permeable, photoluminescent microbatteries embedded in the color filter of a screen. *Energy Environ. Sci.* **11**, 2414–2422 (2018)
169. Jin, Y., Li, S., Kushima, A., et al.: Self-healing SEI enables full-cell cycling of a silicon-majority anode with a coulombic efficiency exceeding 99.9%. *Energy Environ. Sci.* **10**, 580–592 (2017)
170. Chen, S., Gao, Y., Yu, Z., et al.: High capacity of lithium-sulfur batteries at low electrolyte/sulfur ratio enabled by an organosulfide containing electrolyte. *Nano Energy* **31**, 418–423 (2017)
171. Zheng, S., Ma, J., Wu, Z.S., et al.: All-solid-state flexible planar lithium ion micro-capacitors. *Energy Environ. Sci.* **11**, 2001–2009 (2018)
172. Dong, L., Ma, X., Li, Y., et al.: Extremely safe, high-rate and ultralong-life zinc-ion hybrid supercapacitors. *Energy Storage Mater.* **13**, 96–102 (2018)
173. Wang, H., Zhu, C., Chao, D., et al.: Nonaqueous hybrid lithium-ion and sodium-ion capacitors. *Adv. Mater.* **29**, 1702093 (2017)
174. Su, F., Hou, X., Qin, J., et al.: Recent advances and challenges of two-dimensional materials for high-energy and high-power lithium-ion capacitors. *Batter. Supercaps* **3**, 10–29 (2019)
175. Gaikwad, A.M., Khau, B.V., Davies, G., et al.: A high areal capacity flexible lithium-ion battery with a strain-compliant design. *Adv. Energy Mater.* **5**, 1401389 (2015)
176. Xu, Y., Schwab, M.G., Strudwick, A.J., et al.: Screen-printable thin film supercapacitor device utilizing graphene/polyaniline inks. *Adv. Energy Mater.* **3**, 1035–1040 (2013)
177. Huang, Y., Zhong, M., Huang, Y., et al.: A self-healable and highly stretchable supercapacitor based on a dual crosslinked polyelectrolyte. *Nat. Commun.* **6**, 10310 (2015)
178. Xiao, H., Wu, Z.S., Zhou, F., et al.: Stretchable tandem micro-supercapacitors with high voltage output and exceptional mechanical robustness. *Energy Storage Mater.* **13**, 233–240 (2018)
179. Wang, Z.L.: Self-powered nanosensors and nanosystems. *Adv. Mater.* **24**, 280–285 (2012)
180. Zhong, J., Zhang, Y., Zhong, Q., et al.: Fiber-based generator for wearable electronics and mobile medication. *ACS Nano* **8**, 6273–6280 (2014)
181. Guo, R., Chen, J., Yang, B., et al.: In-plane micro-supercapacitors for an integrated device on one piece of paper. *Adv. Funct. Mater.* **27**, 1702394 (2017)
182. Zi, Y., Niu, S., Wang, J., et al.: Standards and figure-of-merits for quantifying the performance of triboelectric nanogenerators. *Nat. Commun.* **6**, 8376 (2015)
183. Bai, L., Zhang, Y., Tong, W., et al.: Graphene for energy storage and conversion: synthesis and interdisciplinary applications. *Energy Rev, Electrochem* (2019). <https://doi.org/10.1007/s41918-41019-00042-41916>



Xiaoyu Shi received his B.S. from Nankai University in 2015 and is currently a Ph.D. candidate at the University of Science and Technology of China under the co-supervision of Prof. Xinhe Bao and Prof. Zhong-Shuai Wu. His current research is focused on printable energy storage devices and integrated systems.



Zhong-Shuai Wu received his Ph.D. from the Institute for Metal Research, CAS, in 2011 and worked as a postdoctoral fellow at the Max Planck Institute for Polymer Research in Mainz, Germany, from 2011 to 2015. Subsequently, Dr. Wu became a full Professor and Group Leader of 2D Materials and Energy Devices at DICP, CAS, and was promoted in 2018 as a DICP Chair Professor. Currently, Prof. Wu's research interests include graphene and 2D materials, surface- and nanoelectrochemistry,

microscale electrochemical energy storage devices, supercapacitors, batteries and catalysis. He is a recipient of the National Natural Science Award (2nd class, 2017), the 2018 and 2019 High Cited Researchers (Clarivate Analytics) and the Fellow of the Royal Society of Chemistry. He is an editor of *Applied Surface Science*, section editor of *Journal of Energy Chemistry* and editorial board of *Energy Storage Materials*, *Journal of Physics: Energy*, and *Physics*.



Xinhe Bao received his Ph.D. in Physical Chemistry from Fudan University in 1987 and held an Alexander von Humboldt Research Fellow position at the Fritz-Haber Institute between 1989 and 1995 as hosted by Prof. Gerhard Ertl. Subsequently, Dr. Bao joined DICP as a full Professor and became a member of the CAS in 2009. Currently, Prof. Bao's research interests include nano and interfacial catalysis with a focus on the fundamental understanding of heterogeneous catalysis, including

the development of novel catalysts and catalytic processes related to energy conversion and storage.